Bitlis Eren University Journal of Science and Technology

Bitlis Eren Üniversitesi Bilim ve Teknoloji Dergisi

Bitlis Eren University Journal of Science and Technology

Yıl/Year: 2022 • Cilt/Volume: 12 • Sayı/Issue: 2

Editorial Board

Bitlis Eren University Journal of Science and Technology (Bitlis Eren Univ J Sci & Technol) is an international, refereed open access electronic journal. Research results, reviews and short communications in the fields of Biology (Medicinal, Molecular and Genetics, Veterinary and Agriculture), Physics, Chemistry, Mathematics and Statistics, and also Engineering Sciences are accepted for review and publication. Papers will be published in English. Scientific quality and scientific significance are the primary criteria for publication. Articles with a suitable balance of practice and theory are preferred. Manuscripts previously published in other journals and as book sections will not be accepted.

Bitlis Eren University Journal of Science and Technology indexed in:
- EBSCO

Articles

Performance of different membership functions in stress classification with fuzzy logic

Mehmet Akif Bülbül ᵃ*, iD

ᵃ Nevsehir Haci Bektas Veli University, Department of Computer Engineering, TR-50300 Nevsehir, Turkey

ARTICLE INFO

ABSTRACT

Stress has become an indispensable part of today's world. Stress can have a very serious negative impact on human health. Knowing the intensity of stress on people is important in order to cope with it. In this study, 4 different Fuzzy Logic (FL) structures were used to classify human stress through sleep. In the established structures, the human stress detection data set in sleep and through sleep obtained from Kaggle was used. In the FL structures created, blood oxygen level and respiratory rate were taken as input and stress classification was made accordingly. Their performance in the classification of sleep stress was evaluated by using different membership functions in 4 different structures. In order to make a fair comparison in the established structures, the FL parameter was determined the same, except for the membership functions. As a result of experimental studies, the F model established with the generalized bell showed more successful results than the models established with other membership functions.

1. Introduction

Stress, which has made a great impact on people from the past to the present and has become a popular disease in the technological age we live in, seriously affects human health (Deveci, 2017). Stress affects vital functions such as heart rate, blood pressure, breathing rate, blood sugar in humans (S. YILDIRIM, 2008). In order to minimize these effects, knowing the stress level is important for taking the right steps. In addition, determining the stress situation requires time and cost. Decision support systems eliminate these disadvantages. Thanks to the developing new generation technologies and artificial intelligence, decision-making models are being developed in many areas (Adem et al., 2019; Bülbül et al., 2022; Bülbül and Öztürk, 2022; Isik et al., 2017; Işık et al., 2018; Pacal and Karaboga, 2021). These developed models can eliminate the disadvantages such as time, cost, and expert person requirements.

Looking at the studies in the literature, Kumar and Dhulipala, in a study they conducted (Kumar and Dhulipala, 2016), made a fuzzy logic-based stress classification as a result of the surveys they conducted on social networking sites. In the study, where blood pressure and heart rate were used as inputs, it was emphasized that devices that can access social networks increase stress. Rasgoo et al. (Rastgoo et al., 2019) proposed a model for classification of drivers' stress.

Successful results have been obtained in stress classification with this model, which uses convolutional neural networks and long short-term memory. Baumgartl et al. (Baumgartl et al., 2020) have proposed a model for diagnosing chronic stress. Random Forest Classifier was used in the model using EEG data. Successful results were obtained as a result of experimental studies. Shin et al. (Shin et al., 2002) used fuzzy logic to predict the stress situation on people. In the study using 5 different biosignals, a model was created that quickly evaluated the stress on humans and tested on healthy individuals. Nagvi et al. (Naqvi et al., 2021) used FL to perform stress measurement. Stress level was measured with the parameters of temperature, oxygen level, blood pressure, skin moisture and heart rate taken with physiological sensors and successful results were obtained. Zalabarria et al. (Zalabarria et al., 2018) used fuzzy logic to classify the stress level in humans. In the study, 3 physiological variables, respiration, galvanic skin response, and electrocardiogram, were used as input and stress was classified into 3 groups.

In the literature, FL is frequently used in stress classification. The studies used are generally based on a single model. There are many membership functions in the FL model. The use of different membership functions on the same model affects the success of the model. In this study, 4 different FL models were used to classify sleep and human stress. Classification successes of models established with different membership functions have been controversially compared.

*Corresponding author. Tel.: +90 364 219 19 19 (3360) fax: +90 364 223 08 04
E-mail address: makifbulbul@nevsehir.edu.tr
ORCID : 0000-0003-4165-0512 (M. A. Bülbül)

2. Material and Method

1.1. Fuzzy logic

FL is a set of objects with uncertain boundaries that are separated from normal sets by the concept of membership (Awasthi et al., 2005). The fuzzy logic structure consists of four basic structures: fuzzification, rule base, inference mechanism and defuzzification (Bülbül et al., 2019). The FL model presented by these structures is shown in Figure 1.
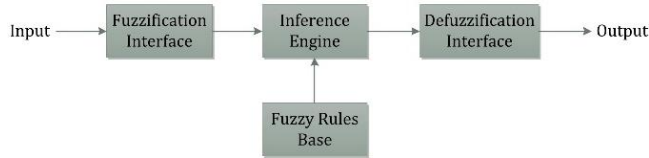

Figure 1. FL structure

In the FL model presented in Figure 1, the data is blurred with the first determined membership function. An inference is obtained according to the rule base determined over the fuzzy data. The resulting inference information is defuzzificationed and the output is obtained (E. YILDIRIM et al., 2021).

1.2. Dataset

The data set used in the study was taken from kaagle and is used in the literature (Human Stress Detection in and through Sleep, n.d.). The data set includes snoring interval, respiratory rate, body temperature, limb movement rate, blood oxygen levels, eye movement, number of sleep hours, heart rate information and stress levels related to these measurements, collected from 630 individuals. Stress levels based on these criteria were classified into 5 groups as low/normal, medium low, medium, medium high, and high (Rachakonda et al., 2021).

1.3. Evaluation metrics

Performance evaluation in multidimensional classifiers can be measured with accuracy calculation (Heydarian et al., 2022). In order to make this calculation, the confusion matrix of the classifier must be created. An exemplary multidimensional confusion matrix is shown in Figure 2.

Figure 2. Multidimensional confusion matrix structure

In Figure 2, TP stands for true positive, FP stands for true negative, TN stands for false positive, and FN stands for false negative. According to these expressions, the accuracy is calculated as presented in Equation 1 (Chen et al., 2022).

$$\text{Accuracy}(Acc) = \frac{TP+TN}{TP+TN+FN+FP} \tag{1}$$

3. Experimental Studies and Results

In this part of the study, FL models were established to classify the stress levels of individuals with Triangle (Model1), Trapezoid (Model2), Generalized Bell (Model3), Gauss (Model4) membership function. For each FL model, respiratory rate (RR) and blood oxygen level (BO) were used as inputs in the data set, while stress level (SL) based on these values was determined as output. The boundary values of the membership functions in FL are as shown in Table 1.

Table 1. Boundary values of the membership functions.

Parameters	Minimum	Maximum
RR (input)	82	97
BO (input)	16	30
SL (output)	0	4

Membership functions are classified as low(L), medium(M), high(H) in each model, and the rule base presented in Table 2 is used in each model for a fair comparison.

Table 2. Rule base used in models.

RR	BO		
	Low	Middle	High
Low	Low	Low	Low
Middle	Middle	Middle	Middle
High	High	High	High

The boundary values of the membership functions created in each model are kept the same for a fair comparison, and the membership functions created in different models for BO are shown in Figure 3.

Each model created was applied on the data set and the output values produced by the models were rounded for the clusters. In the established models, Mamdani inference method and center defuzzification method were used as they are frequently used in the literature with successful results. (Mohapatra and Lenka, 2016) In the Models were created on the MATLAB platform. Confusion matrix created for each model as a result of experimental studies is shown in Table 3-6.
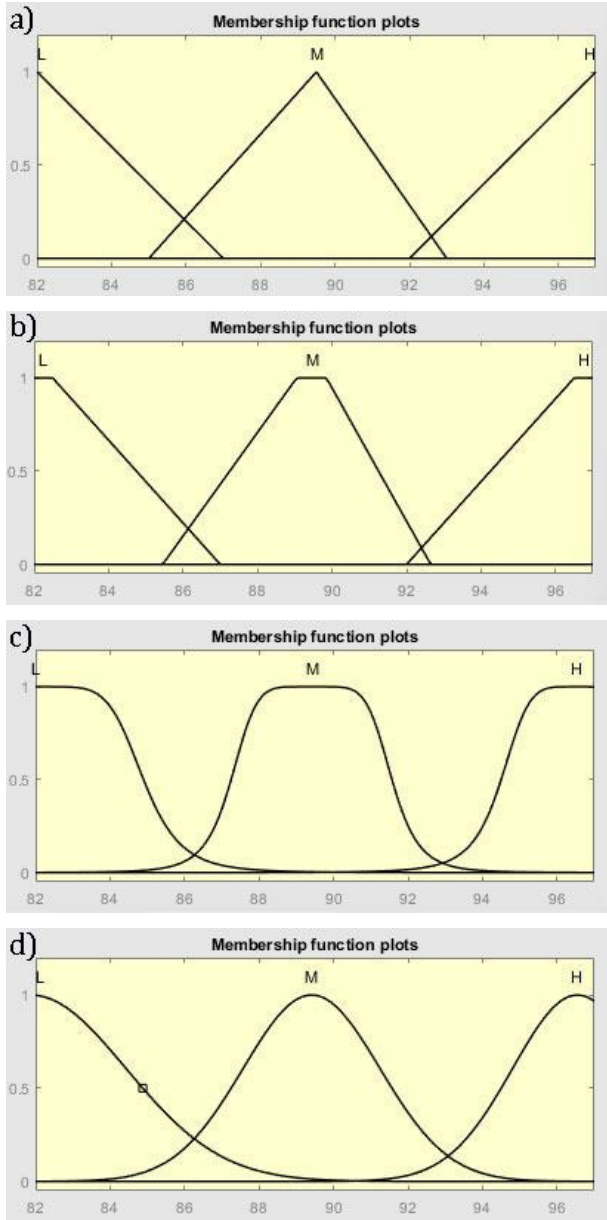
Figure 3. Membership functions used in the study a) Triangle membership function b) Trapezoidal membership function c) Generalized bell membership function d) Gauss membership function

Table 3. Confusion matrix for Model1.

	Predicted Values				
Actual values	Low / Normal	Medium / Low	Medium	Medium / High	High
Low / Normal	126	0	0	0	0
Medium/ Low	0	124	2	0	0
Medium	0	0	122	4	0
Medium/ High	0	0	56	70	0
High	0	0	0	78	48

Table 4. Confusion matrix for Model2.

	Predicted Values				
Actual values	Low / Normal	Medium / Low	Medium	Medium / High	High
Low / Normal	126	0	0	0	0
Medium/ Low	2	116	8	0	0
Medium	0	0	99	27	0
Medium/ High	0	0	59	67	0
High	0	0	0	52	74

Table 5. Confusion matrix for Model3.

	Predicted Values				
Actual values	Low / Normal	Medium / Low	Medium	Medium / High	High
Low / Normal	126	0	0	0	0
Medium/ Low	10	99	17	0	0
Medium	0	0	126	0	0
Medium/ High	0	0	32	94	0
High	0	0	0	33	93

Table 6. Confusion matrix for Model4.

	Predicted Values				
Actual values	Low / Normal	Medium / Low	Medium	Medium / High	High
Low / Normal	126	0	0	0	0
Medium/ Low	0	121	5	0	0
Medium	0	0	126	0	0
Medium/ High	0	0	32	94	0
High	0	0	0	94	32

Using the confusion matrices created in Table 3-6 for each model, the accuracy rates of the models were calculated according to the accuracy formula presented in Equation 1. The success of each model in stress classification is shown in Table 7.

Table 7. Accuracy rates of models.

Models	Accuracy (%)
Model1 (Triangle membership function)	78
Model2 (Trapezoidal membership function)	76
Model3 (Generalized bell membership function)	85
Model4 (Gauss membership function)	79

According to Table 7, the model established with the Generalized Bell membership function produced more successful results in stress classification than other models. In this model, as in other models, the respiratory rate and blood oxygen level were used as inputs, the mamdani method was used in the extraction step, and the centroid method was used in the defuzzification step.

4. Conclusion

Stress, which is an indispensable part of today's world, causes negative and serious problems on human health. The intensity level of the stress on the person is directly proportional to the damage done. Although it is important to know the stress level in order to eliminate stress, decision support systems used in this field are of great importance. In this study, FL-based models were created for the classification of human stress. Experimental studies were carried out on the data set used in the study by choosing different membership functions in the models created. The findings showed that the FL model established with the Generalized Bell membership function gave more successful results than the other models. In future studies, decision support systems can be created on different platforms. With the specified parameters, applications can be developed easily in mobile environments.

References

Adem, K., Kiliçarslan, S., and Cömert, O., 2019. Classification and diagnosis of cervical cancer with stacked autoencoder and softmax classification. Expert Systems With Applications, 115, 557–564. https://doi.org/10.1016/j.eswa.2018.08.050

Awasthi, A. K., Dubey, O. P., Awasthi, A., and Sharma, S., 2005. A fuzzy logic model for estimation of groundwater recharge. Annual Conference of the North American Fuzzy Information Processing Society – NAFIPS, Detroit, MI, USA, 26-28 June, p. 809-813. https://doi.org/10.1109/NAFIPS.2005.1548644

Baumgartl, H., Fezer, E., and Buettner, R. 2020., Two-level classification of chronic stress using machine learning on resting-state EEG recordings. 26th Americas Conference on Information Systems, AMCIS, 15-17 August.

Bülbül, M. A., Harirchian, E., Işık, M. F., Aghakouchaki Hosseini, S. E., and Işık, E., 2022. A Hybrid ANN-GA Model for an Automated Rapid Vulnerability Assessment of Existing RC Buildings. Applied Sciences, 12(10), 5138. https://doi.org/10.3390/app12105138

Bülbül, M. A., and Öztürk, C., 2022. Optimization, Modeling and Implementation of Plant Water Consumption Control Using Genetic Algorithm and Artificial Neural Network in a Hybrid Structure. Arabian Journal for Science and Engineering, 47(2), 2329-2343. https://doi.org/10.1007/s13369-021-06168-4

Bülbül, M. A., Öztürk, C., Ilçi, V., and Ozulu, I. M., 2019. Two-Dimensional Error Estimation in Point Positioning with Fuzzy Logic. 2018 International Conference on Artificial Intelligence and Data Processing IDAP 2018, Malatya-Turkey, 28-30 September, p. 1-4 . https://doi.org/10.1109/IDAP.2018.8620901

Chen, D.,Lu, Y., & Hsu, C. Y., 2022. Measurement Invariance Investigation for Performance of Deep Learning Architectures. IEEE Access, 10: 78070-78087. https://doi.org/10.1109/ACCESS.2022.3192468

Deveci, B., 2017. İş Stresi Ve Turizm İşletmelerinde Yapilan Araştirmalara İlişkin Bir Değerlendirme. Mehmet Akif Ersoy Üniversitesi Sosyal Bilimler Enstitüsü Dergisi, 9(20), 39-53. https://doi.org/10.20875/makusobed.306671

Heydarian M., Doyle, T. E., and Samavi, R., 2022. MLCM: Multi-Label Confusion Matrix. IEEE Access, 10, 19083-19095. https://doi.org/10.1109/ACCESS.2022.3151048

Human Stress Detection in and through Sleep. (n.d.). Retrieved October 17, 2022, from https://www.kaggle.com/datasets/laavanya/human-stress-detection-in-and-through-sleep

Işik, E., Işik, M. F., and Bülbül, M. A., 2017. Web based evaluation of earthquake damages for reinforced concrete buildings. Earthquake and Structures, 13(4), 423-432. https://doi.org/10.12989/eas.2017.13.4.387

Işık, M. F., Işık, E., & Bülbül, M. A., 2018. Application of iOS/Android based assessment and monitoring system for building inventory under seismic impact. Gradjevinar, 70 (12), 1043-1056. https://doi.org/10.14256/JCE.1522.2015

Kumar, M. G. S., and Dhulipala, V. R. S., 2016. Fuzzy Logic Based Stress Level Classification using Physiological Parameters. Asian Journal of Research in Social Sciences and Humanities, 6(cs1), 697-713. https://doi.org/10.5958/2249-7315.2016.00990.4

Mohapatra, A. G., and Lenka, S. K., 2016. Neural network pattern classification and weather dependent fuzzy logic model for irrigation control in WSN based precision agriculture. Procedia Comput. Sci, 78, 499-506. https://doi.org/10.1016/j.procs.2016.02.094

Naqvi, S., Shaikh, A. Z., Altaf, T., and Singh, S., 2021. Fuzzy Logic Enabled Stress Detection Using Physiological Signals. Lecture Notes of the Institute for Computer Sciences, Social-Informatics and Telecommunications Engineering, LNICST, Virtual Event, 04 November p. 161–173. https://doi.org/10.1007/978-3-030-90016-8_11

Pacal, I., and Karaboga, D., 2021. A robust real-time deep learning based automatic polyp detection system. Computers in Biology and Medicine, 134, 104519. https://doi.org/10.1016/j.compbiomed.2021.104519

Rachakonda, L., Bapatla, A. K., Mohanty, S. P., and Kougianos, E., 2021. SaYoPillow: Blockchain-Integrated Privacy-Assured IoMT Framework for Stress Management Considering Sleeping Habits. IEEE Transactions on Consumer Electronics, 67(1), 20-29. https://doi.org/10.1109/TCE.2020.3043683

Rastgoo, M. N., Nakisa, B., Maire, F., Rakotonirainy, A., and Chandran, V., 2019. Automatic driver stress level classification using multimodal deep learning. Expert Systems with Applications, 138, 112793. https://doi.org/10.1016/j.eswa.2019.07.010

Shin, J. W., Seongo, H. M., Cha, D. I., Yoon, Y. R., and Yoon, H. R, 1998. Estimation of stress status using biosignal and fuzzy theory. International Conference of the IEEE Engineering in Medicine and Biology Society, 01 November, Vol. 3 p. 1393-1394. https://doi.org/10.1109/iembs.1998.747141

Yildirim, E., Avci, E., and Yilmaz, B., 2021. Serbest Basinç Dayaniminin Tahmininde Sugeno Bulanik Mantik Yaklaşimi. Uludağ University Journal of The Faculty of Engineering, 26(1), 97-108. https://doi.org/10.17482/uumfd.863121

Yildirim, S., 2008. Muhasebe Öğretim Elemanları ve Meslek Mensuplarının Mesleki Stres Düzeyi Üzerine Bir Araştırma. Muhasebe ve Finansman Dergisi, 38, 153–162.

Zalabarria, U., Irigoyen, E., Martínez, R., and Arechalde, J., 2018. Acquisition and fuzzy processing of physiological signals to obtain human stress level using low cost portable hardware. In International Joint Conference SOCO'17-CISIS'17-ICEUTE'17, León-Spain, 6–8 September, p. 68-78. https://doi.org/10.1007/978-3-319-67180-2_7

Pozzolanic activity of pumice under different curing temperatures and durations

Muhammed TANYILDIZI a,* iD

a Bitlis Eren University, Department of Civil Engineering, TR-13000, Bitlis, Turkey

ARTICLE INFO

ABSTRACT

Objective of the work: This study focused on the investigations of the pozzolanic activity of the pumice under different curing temperatures and durations.

Materials and Method: Pumice powder, standard sand, and slaked lime were used as materials in this study. Within the scope of the study, one mixture design was used following TS 25. In total, 9 different curing regimes such as three different heat cures at 55˚C, 75˚C, and 90˚C and three different curing durations as 7, 14, and 28 days for each curing temperature. Some experimental analyses including compressive strength, flexural strength, and ultrasonic pulse velocity test were conducted to investigate the effect of the curing regimes on the pozzolanic activity of pumice.

Results: The pozzolanic activity of pumice increased to a certain extent with increasing curing temperature and duration. The optimum curing regime obtained for the pozzolanic activity of pumice in this study was curing at 75 ˚C for 28 days, which the highest strength values were obtained with.

1. Introduction

Sustainability is the main concern in societies due to contributing to the persistence of the environment through the preservation of natural sources. Sustainable practices support ecological, human, and economic health by arising environmental consciousness in modern construction works. The enormous amounts of raw materials and energy consumption for manufacturing construction materials are significant factors that are related to sustainability (Elizondo-Martínez et al., 2020; Chandrappa and Biligiri, 2016, URL-1; Alaskar et al., 2021; Karasin et al., 2022; İpek, 2022). These manufacturing processes are also responsible for a significant amount of greenhouse gases released in nature. Concrete is the most used construction material with water owing to its versatility and availability all over the world. Being such a crucial material for the construction industry, the sustainability of concrete has vital importance for societies and sector representatives. The sustainability of concrete is maintained with its constituents, especially with cement which is the foremost ingredient of concrete. However, the production of one ton of Portland cement releases approximately one ton of carbon dioxide (CO_2) and other greenhouse gases. Since cement production consumes a large amount of energy and releases carbon dioxide (CO_2), a greenhouse gas type, into nature in significant amounts, societies and researchers are looking for alternative materials that can be substituted for cement to minimize its usage in concrete, although it is an inevitable ingredient of concrete. Therefore, replacing the cement in the concrete with a more secondary binding material (mineral additive) than general use is one of the most applied and easiest methods to produce more innovative and sustainable concrete (Güneyisi et al., 2014; Justnes and Martius-Hammer, 2015; Naik, 2008; Pereira et al., 2013). Today, pozzolans are used as a substitute material for cement in concrete production. Pozzolans are natural or by-product materials that do not naturally have

* *Corresponding author.* Tel.: +90 434 222 0000-3612 fax: + +90 434 222 91 45
E-mail address: mtanyildizi@beu.edu.tr
ORCID : 0000-0002-8507-2825 (M. Tanyıldızı)

cementitious properties. However, when finely ground, they are siliceous or siliceous and aluminous materials that react with calcium hydroxide, also known as portlandite, in an aqueous medium and exhibit cementitious properties. And, the ability of the active silica in pozzolan to react with calcium hydroxide and water is defined as pozzolanic activity (Massazza, 1993). In addition to silica and aluminum which are the main oxides of pozzolans, they can contain iron oxide, calcium oxide, alkaline, and carbon. The amount of oxides depends on the source of pozzolans. Pozzolans were first used about two thousand years ago during the time of the ancient Romans. In the Italian town of Pozzuoli, volcanic ash was first found by the Romans to be a binding material when mixed with water and slaked lime. They are generally divided into two groups natural and by-product or artificial products. Natural pozzolans are usually obtained with the method of break or ground. Volcanic glasses, volcanic tuffs, trasses, and some clays are types of natural pozzolans. The artificial pozzolans are acquired as by-products from some activities of industry sectors. Silica fume, fly ash and large furnace slag are the most well-known artificial pozzolans. In addition to the utilization of pozzolan as cement substitute material in concrete, they are used to improve workability, minimize segregation, reduce the hydration heat, prevent the detrimental effects of alkali-silica reactions, cut down the permeability, enhance the ultimate strength and increase the durability against sulfate in concrete. When pozzolans and Portland cement mixture are reacting, the free lime (calcium oxide or portlandite) in the cementitious mixture decrease due to the pozzolanic reaction. After a while, there are more calcium-silicate-hydrate (C-S-H) products in mixtures with pozzolans compared to the Portland cement mixtures. Containing more C-S-H gels that have the higher binding characteristic of pozzolanic concretes results in increasing the strength and durability of concrete against environmental effects. How well the reaction between the pozzolan in the concrete mixture and the hydrated lime is determined by the pozzolanic activity. For pozzolans to be used in Portland cement concrete, they must have sufficient pozzolanic activity (Bozkurt and Karaca, 2019; Erdoğan, 2016; Güner and Süme, 2000).

In general, four types of methods are used to determine the pozzolanic activity of a pozzolan. These are:

- Chemical methods
- Physical methods
- Mechanic methods
- Micro-structural methods.

The chemical method is one of the methods for directly determining the pozzolanic activity. The method is used to determine the chemical content of the material. This method is based on determining the change in calcium hydroxide that interacts with active minerals in pozzolans by using chemical titration techniques while the reaction is going on between pozzolan and the cementitious mixture (Bulut and Tanaçan, 2009; Kurugöl, 2017).

In the physical method, the pozzolanic activity is determined by physical changes that occurred in the structure of the pozzolan. The physical changes are determined by measuring the changing in electrical conductivity at various times. Another method of determining the pozzolanic activity with the physical method is to measure the increase in the specific surface of cement in the mixture. And, the mechanic method is based on determining the compressive strength of the mixture.

In micro-structural methods, some methods such as petrographic analysis, electron microscope, differential thermal analysis (DTA), thermogravimetric analysis (TG), X-ray powder diffraction (XRD), X-ray Fluorescence (XRF) are utilized to determine the pozzolanic activity. The petrographic analysis is used to determine the morphology that are resulting from reactions. An electron microscope presents a chance to study cement hydration products in detail. DTA analysis is based on a comparison of the heat given (exothermic) or taken (endothermic) heat when a substance undergoes physical and chemical changes. The endothermic peaks seen in the DTA graph represent the water loss or decomposition, and the exothermic reaction peaks are indicative of representing the formation of a new composition. TG analysis shows the weight loss of material under the effect of heat. Thus, DTA and TG provide to determine the quantity of C-S-H gels and consumed calcium hydroxide. XRD shows the graph of crystalline minerals in the mixture to detect the hydration products. XRF allows to determine the pozzolanic activity by stating the SiO_2, Al_2O_3, Fe_2O_3 oxides as percentage in pozzolan (Bulut and Tanaçan, 2009; Chen, 1984; Joshi, 1970; Kurugöl, 2017).

Pumice is a lightweight aggregate of volcanic origin formed during the solidification of molten lava. The porous nature of pumice is due to the formation of tiny air spaces when the gases in the molten lava are trapped as it cools (Kabay et al., 2015; Yücel et al., 2020). Pumice has been used as an aggregate and/or mineral admixture in the concrete industry (Öz, 2018). The usage of pumice powder (PP) as a natural pozzolan in the cement industry is quite promising for sustainable development (Gencel, 2015). When reviewing the literature, there have been some studies that focused on the pozzolanic activity of pumice under different circumstances. Mboya et al. (2017) examined the pozzolanic activity of cement mixtures with pumice additives and stated that the pozzolanic activity effect of pumice emerged after 28 days of curing and caused an increase in the strength of cement mixtures. Sarıdemir et al. (2016) indicated that the addition of ground pumice in the ratio of 5% increased the compressive strength of high-strength concrete, which was attributed to the cementitious properties of pumice. In their study, Kılıç

and Sertabipoğlu (2015) stated that replacing the cement with natural and heated pumice separately up to 15% had a positive effect on the compressive strength of the cement mortar, which was also attributed to the cementitious properties of the pumice. In addition, the authors reported that the heat treatment (1000°C) applied to pumice significantly affected the pozzolanic activity of pumice, resulting in a much greater increase in the strength of the mortar compared to that of natural pumice. Yu et al. (2020) proved the pozzolanic characteristics of pumice by microstructural and mechanic methods and stated that the pumice satisfies the pozzolanic activity index criteria specified in Chinese Standard JG/T 315. Kabay et al. (2015) stated that replacing cement with pumice powder caused lower mechanical strength at early ages, but increased the strength of pumice at later ages compared to reference concrete, which they attributed to the pozzolanic effect of pumice. This study presented here investigated the pozzolanic activity of pumice under different curing temperatures and durations by mechanic test method following TS 25 (2008) which is a Turkish standard about natural pozzolan (trass) for use in cement and concrete definitions, requirements, and conformity criteria. The X-ray fluorescence (XRF) and X-ray powder diffraction (XRD) were used in the context of the microstructural investigations of the pumice. The compressive strength of specimens was defined for each curing condition to investigate the pozzolanic activity following the TS 25 (2008) standard. However, flexural strength and ultrasonic pulse velocity (UPV) tests were also performed on the test specimens to make comparisons.

2. Experimental Study

2.1. Materials

In this study, pumice obtained from the Bitlis region with a specific gravity of 2.35 was used to produce mortar specimens. The specific surface area of the pumice was 4250 cm²/g. The pumice was ground by the grinder and drought in a drying oven at 105 ± 5 °C until obtaining constant weight. It was prepared in such a way that the amount remaining on the sieve with a 200-micron mesh size would be at most 0.6% by mass, and the amount on the sieve with a 90-micron mesh size would be at the most 8% by mass. The chemical analysis of pumice was determined with the X-ray fluorescence (XRF) method and the mineral phase analysis was conducted with the X-ray powder diffraction (XRD) method. The specific gravity of slaked lime used in this study was 2.40. The slaked lime contained a minimum of 95% CaO and a maximum of 5% MgO. The proportion of slaked slake remained over 45µ was at most 5%. Standard CEN sand with a specific gravity of 2.56 was obtained from Limak Cement Factory to prepare the mortar specimens following the TS EN 196-1 (2016). The grain size distribution of sand is presented in Table 1. Bitlis city mains water, which does not contain harmful organic matter and mineral salts, was used in the production of the mortar samples.

Table 1. Grain size distribution of standard sand.

Aperture size (mm)	Cumulative Remaining %
2,00	0
1,60	7 ± 5
1,00	33 ± 5
0,50	67 ± 5
0,16	87 ± 5
0,08	99 ± 1
Moisture	0.20 %

2.2 Mixture proportioning and curing

The pozzolanic activity test was performed following the standard of TS EN 196-1 (2016) and TS 25 (2018). The required amount of material to prepare three mortar test specimens is given in Table 2. The molds were covered with a 6 mm thick glass plate measuring 210 mm x 185 mm to prevent evaporation after pouring. They were kept at room temperature (23 ± 2) °C for 24 hours. After 24 hours, without removing the molds, they were kept in a drying oven at (55 ± 2) °C for another 6 days. The mortar samples are taken out of the oven and allowed to cool down to room temperature for being ready to test the procedure. At the end of this period of at least 4 hours, the samples are subjected to strength tests. In addition to keeping specimens at 55 ± 2 °C for 6 days referred to as reference specimens in TS 25 (2008), the effect of different curing temperatures and duration was investigated throughout the study. The different curing regimes and Mix IDs are explained in Table 3. For example, P-75-14 means keeping the specimen at room temperature (23 ± 2) °C for 24 hours and after in a drying oven at (75 ± 2) °C for 13 days.

Table 2. Pozzolanic activity test mixture proportions.

Materials	TS 25 (g)	Proportions (g)
Slaked Lime [Ca(OH)₂]	150	150
Pumice	2×150×(S.G* of Pumice/S.G* of Slaked Lime)	294
Standard Sand	1350	1350
Water	0.5×(150+Pumice)	222

S.G: Specific gravity

2.3. Test specimens and methods

Prismatic specimens of 40 × 40 × 160 mm dimensions were produced for testing flexural strength and ultrasonic pulse velocity tests. The compressive strength test was conducted on half specimens obtained after the flexural strength test. The strength tests were conducted by a fully automatic computer-controlled cement compression and flexural test press that is capable of applying loads up to 10 kN and 200 kN for flexural and compressive strength tests respectively following TS EN 196-1 (2016). Each experimental parameter

was determined by averaging the results of three samples. Ultrasonic pulse velocity (UPV) tests were conducted on specimens before the flexural strength test was performed. Strength properties without damaging the test specimen using an ultrasonic pulse velocity device can be obtained. The time it takes for the ultrasonic sound waves sent into the sample to reach the other side of the sample is measured and the wave velocity is calculated. With this wave velocity, the strength properties of the sample can be estimated. After determining the time taken for the sound waves sent from one end of the sample to reach the other end during the experiment, the wave velocity is calculated with the following formula (Cosmes-López et al., 2017; Demirhan et al., 2019; Massazza, 1993):

$$V = \frac{S}{t} \times 10^3 \tag{1}$$

Where;

V= Ultrasonic pulse velocity (m/s)

S= The Distance between the two ends of the sample (m)

t= Time taken by the pulse to go through (microseconds).

The microstructural analyses including XRF and XRD were conducted on the ground pumice specimen. The XRF analysis was performed at Kastamonu University Central Research Laboratory by Spectro-Xepos II device. The XRF spectroscopy provides the opportunity to determine elemental composition (URL-2). The XRD analysis was made on the specimen to investigate the crystal structure and phase analysis of pumice at Bingöl University Central Laboratory Application and Research Center by Rigaku Ultima IV device (URL-3).

Table 3. The curing regimes and Mixture ID.

Temperature (°C)	Mixture Proportions	Curing duration (days)	Mix ID
55 °C		7	P-55-7
55 °C		14	P-55-14
55 °C		28	P-55-28
75 °C	Mixture proportions given in Table 2	7	P-75-7
75 °C		14	P-75-14
75 °C		28	P-75-28
90 °C		7	P-90-7
90 °C		14	P-90-14
90 °C		28	P-90-28

3. Results and Discussion

3.1. Microstructural analysis

The chemical analysis of pumice was submitted in Table 4. TS 25 (2008) states that the total amount of (SiO_2 + Al_2O_3 + Fe_2O_3) of a natural pozzolan must be at least 70% by mass. And, the amount of SO_3 and Cl must be at most 3% and 0.1% respectively. When Table 5 is analyzed, it is seen that pumice meets these criteria. The pumice sample used in this study obtained from the Bitlis region has a similar chemical composition to the samples taken from other pumice deposits in Turkey presented in the literature such as Nevşehir (Tolğay

et al., 2004), Isparta Gelincik (Kalay, 2010), Manisa Kula (Coşan, 2016), Kayseri (Gündüz and Yılmaz, 1998) and İzmir Menderes (Aksay, 2005) as summarized in Table 5. When analyzing Table 5, it was seen that in general pumice specimens have a total percentage of $SiO_2+Al_2O_3+Fe_2O_3$ oxides between 80% and 90% except that of Manisa Kula. Therefore, the pumice obtained from Manisa Kula can show higher pozzolanic activity.

Table 4. Chemical compositions of Pumice.

Chemical Analysis, (%)	TS 25	Pumice
Na_2O	-	7.87
MgO	-	0.03
SiO_2		72.06
Al_2O_3	≥70	11.83
Fe_2O_3		3.91
P_2O_5	-	0.01
SO_3	≤ 3.0	0.01
Cl	≤ 0.1	0.06
K_2O	-	3.70
CaO	-	0.44
MnO	-	0.08

Table 5. The ($SiO_2+Al_2O_3+Fe_2O_3$) oxides comparison of pumice specimens from different regions in Turkey.

Pumice Origin	($SiO_2+Al_2O_3+Fe_2O_3$) (%)
Bitlis	87.80
Nevşehir (Tolğay et al., 2004)	88.32
Isparta Gelincik (Kalay, 2010)	81.20
Manisa Kula (Coşan, 2016)	95.17
Kayseri (Gündüz and Yılmaz, 1998)	86.50
İzmir Menderes (Aksay, 2005)	87.14

The XRD pattern of the pumice is presented in Fig. 1. The pumice was found that it has a very broad reflection (peak) between 20° and 30° confirming the presence of the amorphous nature of this material. In addition, the main crystalline mineral phases were identified as albite-calcian, anorthoclase, and quartz.
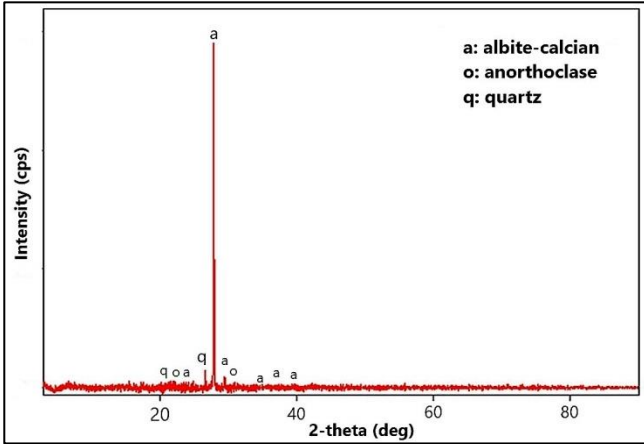
Figure 1. The X-ray diffraction pattern of pumice.

3.2. Strength tests and UPV analyses

The strength tests and UPV analysis results are presented in Table 6. The TS 25 (2008) standard states that the mixture prepared with natural pozzolan and lime must have a compressive strength of at least 4 MPa to meet the pozzolanic activity criteria after curing at room temperature (23 ± 2) °C for 24 hours and at 55 ± 2 °C for 6 days. In the TS 25 standard published in 1975 and repealed, the flexural test criterion was also specified among the pozzolanic activity tests, as well as the compression test, and the flexural strength of the sample was requested to be at least 1 MPa. However, in the current standard of TS 25 (2008), this criterion is no longer required. Although it is not specified in the standard, to make a comparison, the flexural strength tests were performed in the context of this study. On the other hand, the UPV values of specimens were conducted to support the strength test results. When Table 5 is analyzed, it is seen that the maximum compressive and flexural strength was obtained with P-75-28 ID specimen as 8.90 MPa and 2.13 MPa, respectively. Also, the highest UPV value was obtained with this specimen as 3799 m/s. The lowest compressive and flexural strength results were obtained with a specimen of P-55-7 ID as 6.48 MPa and 1.77 MPa, respectively. In addition, the lowest UPV value was obtained for the same specimen as 2450 m/s. It is concluded from Table 5 that, increasing both curing temperature and duration increases the strength of the specimen up to a level. This was attributed to the increase of the pozzolanic reactions with temperature and exposure time. Increasing pozzolanic reactions means producing more C-S-H gel by consuming calcium hydroxide. However, an excessive increase in curing temperature can result in a decrease in strength as seen in curing at 90 °C in Table 5, which has been attributed to lower UPV values, i.e. damage to the microstructure, as seen in the table, meaning an increase in void formation. The pozzolanic activities of pumice under different curing durations and temperatures based on compressive strength are presented in Fig. 2. The change in flexural strength and UPV values of mixtures under different curing durations and temperatures are demonstrated in Fig. 3 and Fig. 4 respectively.

In a similar study conducted to reveal the pozzolanic activity of perlite, it was stated that as the curing duration increased, the pozzolanic activity increased, however, it was affected adversely by the increase of curing temperature from 55°C to 65°C. When comparing the pozzolanic activity of perlite and

pumice based on compressive strength specimens cured at 55 °C for 7 days, it was revealed that perlite had compressive strength approximately 62.04% higher than that of pumice (Bulut and Tanaçan, 2009). In another study, Baki et al. (2019) investigated the pozzolanic activity of rhyolite, fly ash, trachyte, and blast furnace slag for 7 days at 55 °C and found approximately 7, 7.2, 8.2, and 8.6 MPa, respectively. This means each of them shows higher pozzolanic activity than pumice.

Table 6. The strength tests and UPV analyses results.

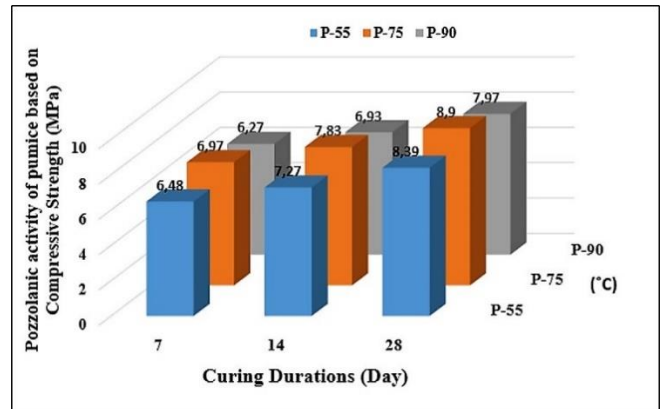| Mixture ID	Compressive Strength (MPa)	Flexural Strength (MPa)	UPV(m/s)
P-55-7	6.48	1.77	3450
P-55-14	7.27	1.83	3573
P-55-28	8.39	1.98	3628
P-75-7	6.97	1.89	3475
P-75-14	7.83	2.01	3684
P-75-28	8.90	2.13	3799
P-90-7	6.27	1.76	3387
P-90-14	6.12	1.73	3361
P-90-28	6.01	1.68	3302

Figure 2. Change in pozzolanic activity of pumice under different curing durations and temperatures based on compressive strength.
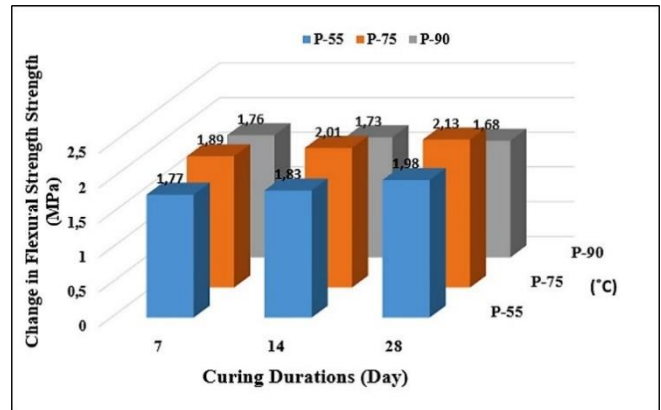

Figure 3. Change in flexural strength of mixtures under different curing durations and temperatures.
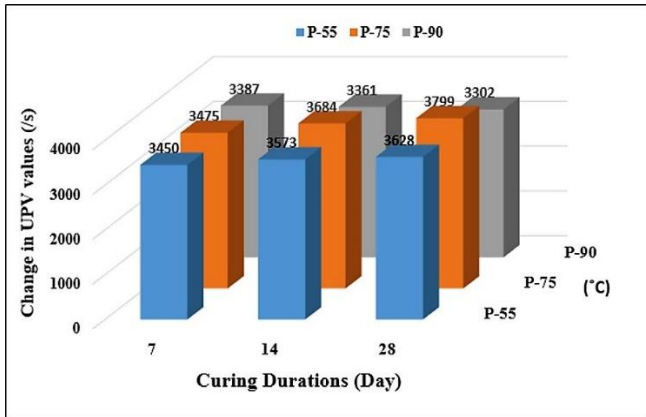
Figure 4. Change in UPV values of mixtures under different curing durations and temperatures.

4. Conclusions

The pozzolanic activity of pumice was affected by both curing temperature and duration. Increasing the curing temperature from 55°C to 75°C caused an increase in the strength of the mortar prepared with pumice powder. With the prolongation of the curing duration, the strength properties of the mortars have also improved. However, increasing the curing temperature up to 90°C resulted in a decrease in the strength properties of mortars. In addition, the results also showed that the strength of mortars decreased with increasing curing duration at 90°C. These results were attributed to the increase in the pozzolanic activity of pumice up to a certain curing temperature and duration, which means producing more C-S-H gels with consuming calcium hydroxide. Moreover, increasing the temperature after a certain level caused a reduction in the strength properties, which was attributed to the damage of the excessive temperature to the microstructure. Based on the findings, it will be useful to determine the possibilities of developing pumice as a building material by using its pozzolanic characteristics at different temperatures and using it together with binders such as cement and lime.

References

Alaskar, A., Alabduljabbar, H., Mohamed, A.M., Alrshoudi, F., and Alyusef, R., 2021. Abrasion and skid resistance of concrete containing waste polypropylene fibers and palm oil fuel ash as pavement material. Construction and Building Materials, 282. https://doi.org/10.1016/j.conbuildmat.2021.122681

Baki, V.A., Nayır, S., Erdoğdu, Ş., and Ustabaş, İ., 2019. Determination of the Pozzolanic Activities of Trachyte and Rhyolite and Comparison of the Test Methods Implemented. International Journal of Civil Engineering. 18(9), 1053–66. DOI: 10.1007/s40999-020-00516-5.

Bozkurt, N., and Karaca, E.O., 2019. The Investigation of Strength and Durability Properties of Mortars Produced with Waste Stone Dusts. Fırat University Journal of Engineering Sciences, 31(1), 11-20.

Bulut, Ü., and Tanaçan, L., 2009. Perlitin Puzolanik Aktivitesi. İtü Dergisi, 8(1).

Chandrappa, A.K., and Biligiri, K.P., 2016. Pervious concrete as a sustainable pavement material Research findings and future prospects: A state-of-the-art review. Construction and Building Materials, 111, 262-274.

Chen, S.S., 1984. Correlation of Fly Ash Characteristics with

Pozzolanic Behavior, Dissertation Partial Satisfaction of the Requirements for The Degree of Doctor of Philosophy in Engineering in The Graduate Division of the University of California, Berkeley, 1-57.

Cosmez-Lopez, M.F., Castellanos, F., and Cano-Barrita, P.F.D.J., 2017. Ultrasound frequency analysis for identification of aggregates and cement paste in concrete. Ultrasonics, 73, 88-95.

Demirhan, S., Türk, K., and Ulugerger, K., 2019. Fresh and hardened properties of self consolidating Portland limestone cement mortars: Effect of high volume limestone powder replaced by cement. Construction and Building Materials, 196, 115-125. DOI: 10.1016/j.conbuildmat.2018.11.111.

Aksay, E.K., 2005. Determination of The Technological Properties of the Izmir-Menderes Pumice Ores as an Industrial Mineral. Dokuz Eylül University, Graduate School of Natural and Applied Sciences, Doctoral Thesis.

Elizondo-Martinez, E.J., Andres –Valeri, V.C., Jato-Espino, D., and Rodriguez-Hernandez, J., 2020. Review of porous concrete as multifunctional and sustainable pavement. Journal of Building Engineering, 27. DOI: 10.1016/j.jobe.2019.100967.

Erdoğan, T.Y, 2016. Concrete. 6th ed. ODTÜ Publication, Ankara. (in Turkish).

Coşan, F.Ş., 2016. The Engineering Properties of High Plasticity Clay Improved by Using Amorphous Silica, Volcanic Tuff and Lime. Süleyman Demirel University Graduate School of Natural and Applied Sciences Department of Construction, Master Thesis.

Gencel, O., 2015. Characteristics of fired clay bricks with pumice additive. Energy and Buildings, 102, 217-224.

Gündüz, L., and Yılmaz, İ., 2001. Orta Anadolu Pomza Oluşumlarının Endüstriyel Olarak Kullanılabilirlik Ölçütleri. Türkiye 17 Uluslararası Madencilik Kongresi ve Sergisi.

Güner, M.S., and Süme, V., 2000. Construction Material and Concrete. 2nd ed. Aktif Publiser, İstanbul. (in Turkish)

Güneyisi, E., Gesoğlu, M., Akoi, A.O.M., and Mermerdaş, K., 2014. Combined effect of steel fiber and metakaolin incorporation on mechanical properties of concrete. Composites Part B: Engineering, 56, 83-91. https://doi.org/10.1016/j.compositesb.2013.08.002

İpek, S., 2022. Macro and micro characteristics of eco-friendly fly ash-based geopolymer composites made of different types of recycled sand. Journal of Building Engineering, 52. https://doi.org/10.1016/j.jobe.2022.104431

Joshi, R.C., 1970. Pozzolanic Reactions in Synthetic Fly Ashes, A Dissertation Submitted to the Graduate Faculty in Partial Fulfillment of the Requirements for the Degree of Doctor of Philisophy, Lowa State University, Ames, Lowa, 1-215.

Justnes, H., and Hammer, T.A.M., 2015. Sustainability – A driver for concrete innovation. XVII ERMCO (European Ready Mixed Concrete Organization) CongressAt: Istanbul, Turkey, v. 1.

N. Kabay N., Tüfekçi M.M, Kızılkanat A.B., and Oktay D., 2015. Properties of concrete with pumice powder and fly ash as cement replacement materials, Construction and Building Materials, 85, 1-8.

Kalay, E., 2010. Using Pumice, Marble Dust and Lime for Stabilization of Compacted High Plasticity Clay. Süleyman Demirel University Graduate School of Applied and Natural Sciences Department of Civil Engineering, Master Thesis.

Karasin, A., Hadzima-Nyarko, M., Işık, A., Doğruyol, M., Karasin, İ.B., and Czarnecki, S., 2022. The Effect of Basalt Aggregates and Mineral Admixtures on the Mechanical Properties of Concrete Exposed to Sulphate Attacks. Materials, 15, 1581. DOI: 10.3390/ma15041581.

Kılıç, A., and Sertabipoğlu, Z., 2015. Effect of heat treatment on pozzolanic activity of volcanic pumice used as cementitious material,

Cement & Concrete Composites, 57, 128-132. DOI: 10.1016/j.cemconcomp.2014.12.006.

Kurugöl, S., 2017. Puzzolanic Activity Detection Procedure: Physical Methods. Cumhuriyet University Faculty of Science Science Journal (CSJ), 38 (1).

F, Massazza., 1993. Pozzolanic Cements. Cement and Concrete Composites, 15, 185-214. DOI: 10.1016/0958-9465(93)90023-3.

Mboya, H.A., King'ondu, C.K., Njau, K.N., and Mrema, A.L., 2017. Measurement of Pozzolanic Activity Index of Scoria, Pumice, and Rice Husk Ash as Potential Supplementary Cementitious Materials for Portland Cement. Advances in Civil Engineering, 2017. DOI: 10.1155/2017/6952645.

Naik, T.R., 2008. Sustainability of Concrete Construction. Practice Periodical on Structural Design and Construction, 13, 2. DOI: 10.1061/(ASCE)1084-0680(2008)13:2(98).

Öz, H.Ö., 2018. Properties of pervious concretes partially incorporating acidic pumice as coarse aggregate. Construction and Building Materials, 166, 601-609. DOI: 10.1016/j.conbuildmat.2018.02.010.

Pereira, C.L., Savastano, H., Paya, J., Santos, S.F., Borrachero , M.V., Monzo, J., and Soriano, L, 2013. Use of highly reactive rice husk ash in the production of cement matrix reinforced with Green coconut fiber. Industrial Crops and Products., 49, 88-96. DOI: 10.1016/j.indcrop.2013.04.038.

Saridemir, M., Severcan, M.H., Ciflikli, M., Celikten, S., Ozcan, F., and Atis, C.D., 2016. The influence of elevated temperature on strength and microstructure of high strength concrete containing ground pumice and metakaolin. Construction and Building Materials, 124, 244-257. DOI: 10.1016/j.conbuildmat.2016.07.109.

Tolğay, A., Yaşar, E., and Erdoğan, Y., 2004. Nevşehir Pomzasınm Agrega Olarak Betonda Kullanılabilirliğinin Araştırılması. 5. Endüstriyel Hammaddeler Sempozyumu, 13-14 Mayıs, İzmir, Türkiye.

TS 25, 2008. Natural pozzolan (Trass) for use in cement and concrete -Definitions, requirements and conformity criteria. Turkish Standard Institution, TSE, Ankara, Turkey.

TS EN 196-1. Methods of testing cement - Part 1: Determination of strength. Turkish Standard Institution, TSE, Ankara, Turkey.

URL-1: https://bumlab.bingol.edu.tr/ (Date of access: 27.11.2022).

URL-2:http://merlab.kastamonu.edu.tr/ (Date of access: 24.11.2022).

URL-3:https://www.sustain.ucla.edu/what-is-sustainability (Date of access: 05.10.2022).

Yu, L., Zhou, S., and Dong, J., 2020. Investigation into Pozzolanic Activity Component of Basalt and Pumice. Journal of Materials in Civil Engineering, 32(6).

Yücel, H.E., Öz, H.Ö., and Güneş, M., 2020. The Effects of Acidic and Basic Pumice on Physico-Mechanical and Durability Properties of Self-Compacting Concretes. Green Building & Construction Economics, 1. DOI: 10.37256/gbce.112020591.

Investigation of thermal performance of newly multilayer wall/roof constructions for low-carbon buildings

Zeki Argunhan [a],* (iD) , Hasan Oktay [b] (iD)

[a] Bitlis Eren University, Department of Mechanical Engineering, TR-13000, Bitlis, Turkey

[b] Batman University, Department of Mechanical Engineering, TR-72100, Batman, Turkey

ABSTRACT

Increasing concerns about energy consumption for heating and cooling of buildings have made it necessary to improve the thermal performance of building materials. However, in addition to using materials with high insulation characteristics, an accurate calculation of the capacities of the heating and cooling systems is also an important factor in ensuring high energy efficiency for low-carbon buildings. The devices will not be selected at capacities larger than the capacities that should be on this point and energy wastage will be prevented. To achieve this goal, in this study, investigations are carried out to produce new concrete types with high thermal insulating characteristics. Besides, many new concrete wall and roof samples were produced with different types of aggregates at different volume ratios and their thermophysical characteristics are tested in accordance with ASTM and EN standards. To estimate the thermal performance of produced samples, a periodic solution method, the Complex Finite Fourier Transform technique, is developed by using thermophysical characteristics data of those structures. The results showed that the daily heat gain values were calculated as 65.909 W/m^2 for the EPC50 wall and 11.324 W/m^2 for the PC40-EPC60 wall with 20 cm thicknesses.

1. Introduction

Increasing energy consumption in parallel with population growth and the rapid depletion of existing energy resources have become a threat to the world. However, the amount of energy required for heating and cooling of buildings has a significant proportion of total energy consumption, and this ratio corresponds to approximately 37% in Turkey (Ozbalta, 2010). The amount of energy consumption increases proportionally with population growth, industrialization, urbanization, etc. However, due to its limited local energy resources, Turkey imports around 75% of the energy it needs from foreign countries. This situation necessitates energy saving and efficient use of energy in our country (Erdal *et al.*, 2008). By the way, it has been determined that 85% energy saving is achieved depending on the places where thermal insulation is applied (TMMOB, 2005). Therefore, it is extremely important for low-carbon buildings that the constructions have high thermal insulation properties. In our country, it is of great importance to developing domestic, low-density, and inflammable materials with high insulation properties. This will ensure efficient use of energy.

Although concrete is the most used, universal, and economical building material in building structures (Think harder concrete, 2013), the places where heat loss is the highest are concrete beams and walls. Buildings' energy consumption should be reduced as much as possible by enhancing their thermal properties. Since aggregates constitute the highest amount of concrete by volume, the components most affect its thermal, sound, and mechanical properties. Lightweight concrete can be produced by using lightweight and porous aggregates in concrete production. Concrete blocks produced from lightweight aggregates; low density, high insulation, fire resistance, heat shock resistance, etc. are the most important advantages of these structures. In many studies, it has been found that lightweight concrete has better insulation than conventional concrete (ACI Committee 122, 2002; Vaou and Panias, 2010; Real et al., 2021; Uysal et al., 2004; Demirboğa et al., 2004) which is due to the porosity of lightweight aggregates (Chandra et al., 2002; Argunhan et al., 2017; Oktay et al., 2015), but also provides the necessary mechanical properties (Bouguerra et al., 1998). Because they are exposed to climatic factors including convection and solar heat flux, the exterior surfaces of the buildings account for a significant portion of the overall cooling load. In addition to the use of building materials with high insulating properties, an accurate calculation of the

* *Corresponding author.* Tel.: +90 434 222 00 30 ; fax: +90 424 222 01 01
E-mail address: zargunhan@beu.edu.tr
ORCID : *0000-0002 3349 3409 (Z. Argunhan), 0000-0002 0917 7844 (H. Oktay)*

capacities of heating and cooling systems is an essential task for low-carbon buildings. In this way, this waste of energy is prevented by not selecting devices with capacities larger than the required ones. However, due to the thermal storage effects of the building mass and the constantly changing external conditions, an accurate assessment of the cooling load is quite difficult and time-consuming (Bansal et al., 2008).

The thermal inertia of a building can be calculated using a variety of techniques (ASHRAE, 1993; De Rosa et al., 2016; Naji et al., 2019). Different analytical techniques, including the separation of variables, the orthogonal extension approach, Green's function, the Laplace transform, and integral procedures have been defined by Özışık and Hahn (2012). In another study, Ulgen (2002) investigated the thermal responses of various wall configurations under the influence of solar radiation experimentally and analytically. Additionally, Yumrutaş et al. (2007) developed a theoretical approach based on the periodic solution of the one-dimensional transient heat transfer issue in buildings for three different wall types and flat roofs, which is commonly used to calculate TETD values.

In the present study, both experimental and theoretical studies are performed. In the experimental study, new wall/roof materials with high thermal insulation properties, which are formed with materials such as perlite and pumice, which our country has world-class reserves in terms of resource maintenance, were produced. In the theoretical study, an analytical solution was developed to calculate the heat gain through the walls and to estimate the thermal performance of produced new lightweight wall elements. To determine the temperature distribution for multilayer wall or flat roof constructions, the calculation approach for the heat gain is based on a solution to the transient heat transfer problem.

2. Material compositions and test methods

The new building's wall and roof components were made from a variety of materials which were locally available ordinary Portland cement (PC), silica fume (SF), fine aggregate, coarse aggregate, rubber aggregate (RA), pumice aggregate (PA), expanded perlite aggregate (EPA), and superplasticizer (SP). Concrete mixtures were designed with an effective water/cement ratio of 0.48 and a total cement amount of 350 kg/m³. Natural aggregates were replaced by expanded perlite, waste tire, and pumice aggregates with fractions between 0% and 100% of the total aggregate volume to produce lightweight concrete samples. Due to insufficient mechanical strength for the concretes formed with the waste rubber and expanded perlite aggregates in volume ratios of 70% and higher, they were not included in this study.

Several tests were conducted on the produced concretes regarding the compressive strengths, bulk density, thermal conductivity, specific heat, and thermal diffusivity according to the ASTM and EN standards. The measurements of the thermal conductivity, specific heat capacity, and thermal diffusivity are performed by TPS (Transient Plane Source) technique (Figure 1.). In the TPS method, the heat is generated by a hot disc composed of a bifilar spiral, which also acts as a sensor for the rise in sample temperature. The benefit of transient methods over stationary or steady-state techniques is that some of them can provide a complete set of thermophysical characteristics in a single quick measurement.

Figure 1. The thermal properties analyzer device

Both mechanical and thermophysical property test results for the produced samples are presented in Table 1.

3. Solution of the transient heat transfer problem and computational procedure

To decide whether any one of the building wall/roof elements is the best performance by the heat transfer, it is necessary to compare heat gain or loss for these elements. Any wall types with lower heat gain values are recommended to applicants in low-carbon buildings. Since the smallest amount of energy is needed to heating and cooling any given space, it is crucial for pollution prevention, humanity, and environmental preservation.

Table 1. Mechanical and thermophysical property of samples

Sample	σ_c (Mpa)	λ(W/m.K)	ρ_k (kg/m³)	c_p (J/kg.K)	α (m²/s)
NC	61.52	2.075	2434.30	630.57	1.35×10^{-6}
EPC10	26.72	1.597	2065.56	776.59	9.95×10^{-7}
EPC20	19.68	1.140	1872.29	799.34	7.62×10^{-7}
EPC30	13.13	0.944	1751.14	817.87	6.59×10^{-7}
EPC40	11.54	0.820	1636.37	828.05	6.05×10^{-7}
EPC50	10.38	0.709	1449.40	918.69	5.32×10^{-7}
EPC60	6.43	0.520	1342.44	961.83	4.02×10^{-7}
PC20	26.75	1.390	2107.30	809.88	8.14×10^{-7}
PC40	18.14	1.060	1888.18	835.89	6.72×10^{-7}
PC50	17.37	0.911	1748.85	881.02	5.91×10^{-7}
PC60	13.32	0.639	1529.34	968.00	4.32×10^{-7}
PC80	11.83	0.421	1350.55	1049.94	2.97×10^{-7}
PC100	9.35	0.358	1112.25	1186.79	2.71×10^{-7}
RC10	35.03	1.720	2224.09	727.94	1.06×10^{-6}
RC20	19.90	1.417	2122.88	754.50	8.84×10^{-7}
RC30	10.39	1.070	1920.16	766.76	7.27×10^{-7}
RC40	6.24	0.829	1805.82	786.68	5.84×10^{-7}
RC50	4.47	0.722	1782.13	824.86	4.91×10^{-7}
RC60	2.94	0.548	1658.99	914.53	3.61×10^{-7}
EPC40-PC60	7.68	0.193	815.92	1189.46	1.99×10^{-7}
EPC50-PC50	5.89	0.158	726.14	1160.03	1.88×10^{-7}
EPC60-PC40	4.47	0.141	693.55	1122.26	1.81×10^{-7}

A mathematical formulation and boundary conditions are used to design a one-dimensional periodic heat transfer problem for a wall or roof component. The temperature of the inner

surfaces of the building walls is determined using the problem's solution.

$$\frac{\partial^2 T_n}{\partial x^2_n} = \frac{1}{\alpha_n}\frac{\partial T_n}{\partial t} \qquad\qquad 1 \le n \le N \qquad (1)$$

$$h_i(T_r - T_1) = -\lambda_1\frac{\partial T_1}{\partial x_1} \qquad\qquad \text{at } x_1 = 0 \qquad (2)$$

$$-\lambda_{n-1}\frac{\partial T_{n-1}}{\partial x_{n-1}}(x_{n-1} = L_{n-1}) = -\lambda_n\frac{\partial T_n}{\partial x_n}(x_n = 0)\ \ 2 \le n \le N \quad (3)$$

$$T(x_{n-1} = L_{n-1}) = T(x_n = 0) \qquad \text{for } 2 \le n \le N \qquad (4)$$

$$-\lambda_N\frac{\partial T_N}{\partial x_N} = h_o[T_N - T_e(t)] \qquad \text{at } x_N = L_N \qquad (5)$$

$$T_e(t) = T_a(t) + \frac{\alpha_s I_t(t)}{h_o} - \frac{\varepsilon\Delta R}{h_o} \qquad \text{at } x_N = L_N \qquad (6)$$

$$I_T(t) = I_b(t)R_b + I_d(t)\left(\frac{1+\cos\beta}{2}\right) + I(t)\rho_g\left(\frac{1-\cos\beta}{2}\right) \qquad (7)$$

$$R_b = \frac{\cos\delta\sin\varphi\cos\gamma\cos\omega + \cos\delta\sin\gamma\sin\omega - \sin\delta\cos\varphi\cos\gamma}{\cos\varphi\cos\delta\cos\omega + \sin\varphi\sin\delta} \qquad (8)$$

$$T_n(z_n, \tau) = \sum_{j=-M}^{M} T_{nj}(z_n) e^{i\omega_j\tau} \qquad \omega_j = 2\pi j \qquad (9)$$

The periodic solution equation for the temperature distribution in a wall, given by Eq. (9), $T_n(z_n, \tau)$ is obtained as a function of the solar energy flux, $I_T(t)$, and ambient air temperature, $T_a(t)$. It is necessary to calculate solar radiation incidents on the structures to obtain temperature variation in the walls and flat roofs. $I_T(t)$ is the hourly solar heat flux on a tilted surface, which is equal to the intensity of solar radiation falling on unit area flux. It can also be expressed as the total of the beam, diffuse, and reflected radiation, given by Duffie and Backman (Duffie and Beckman, 1980).

A function of the interior surface temperatures of the building wall, the interior design air temperature, and the convective heat transfer coefficient is used to calculate the amount of heat gain through any wall. In other words, it may be determined by multiplying the temperature difference by the convection coefficient. As a result, the heat gain can be written as:

$$q_c = h_i[T_1(0,t) - T_r] \qquad (10)$$

The temperature difference shows the temperature difference between the inside surface of the wall $T_1(0, t)$ and interior air temperature, T_r which is commonly taken as 25 °C for the whole cooling season.
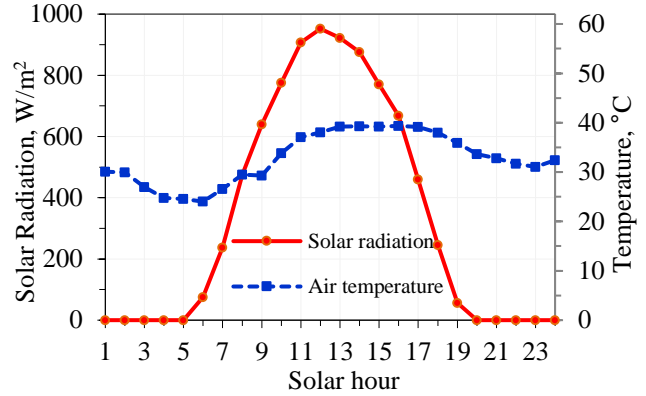

Figure 2. The hourly solar radiation incident and ambient temperature values

The detailed solution to the problem is presented in Ref. (Oktay et al., 2020) in detail. Hence, a computer program in MATLAB was prepared by using climatic data and thermophysical properties of the produced samples. The climatic data are hourly ambient air temperature and solar radiation on a horizontal surface which are measured with the meteorology system established at Batman University on July 26, 2016 given in Figure 2. The inner combined heat transfer coefficients and outer surfaces are taken as 9 and 22 W/m² °C, respectively. Solar absorptivity αs, which depends on the exterior surface color of a building envelope. The algorithm of the program is shown in Figure 3.
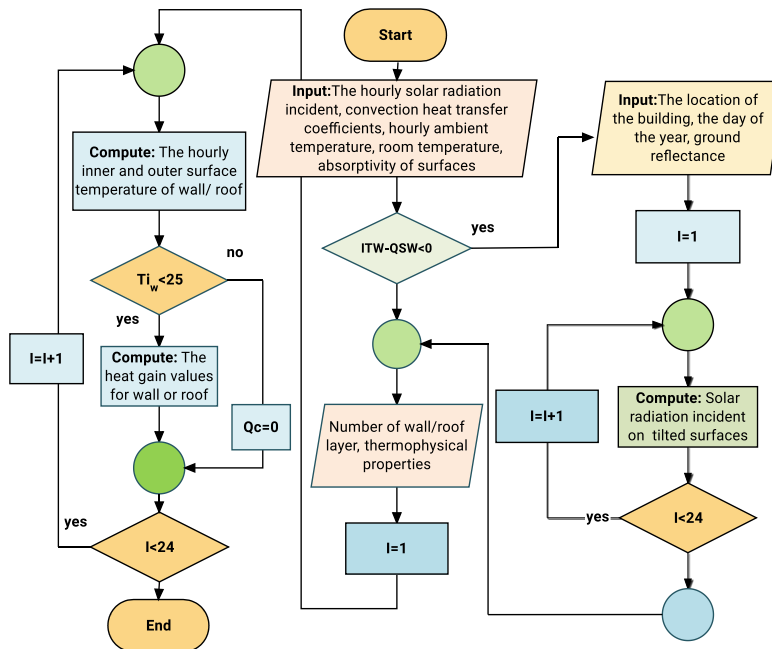

Figure 3. Algorithm of the program in MATLAB

In the program, the hourly air temperature and solar incident values were given as input data. When the program was executed, the type of wall/roof, the number of layers, and their thickness were given as input parameters. Firstly, the hourly sol-air temperature was calculated by using the procedure given in Eq. (6). Then, the inner surface temperature of the wall and the heat gain values were computed as given in Eqs. (9) and (10), respectively.

4. Results and discussions

In this section, an analytical method, the complex finite Fourier transform (CFFT) is obtained by using the thermal performance analysis of lightweight concrete samples. As stated before, the heat gain values passing for the walls/roofs were taken as a reference to compare the thermal performances of the buildings. The schematic representation and dimensions of the walls and flat roofs used in the study are given in Figure 4.
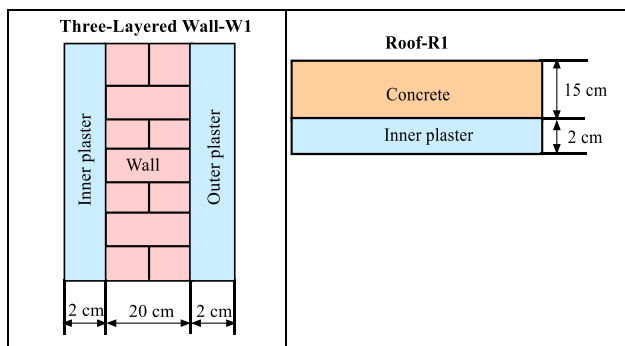

Figure 4. Schematic presentation of a multilayer wall/roof construction.

The heat gain values depending on the East, West, North, and South directions of the EPC50 wall are shown in Figure 5. This is essential for determining the wall constructions' highest heat gain. The heat gain values range from 9 to 10 hours for the lowest values to 20 to 21 hours for the greatest values in all directions. The north wall experienced the lowest daily average heat gain, calculated as 1.624 W/m², while the west wall experienced the highest daily average heat gain, calculated as 17.846 W/m².Since the cooling load of a building element depends on the heat gain and the West side has the most heat gain, it is recommended to designers that the area of the wall due to the West should be minimized for the building located in this region.
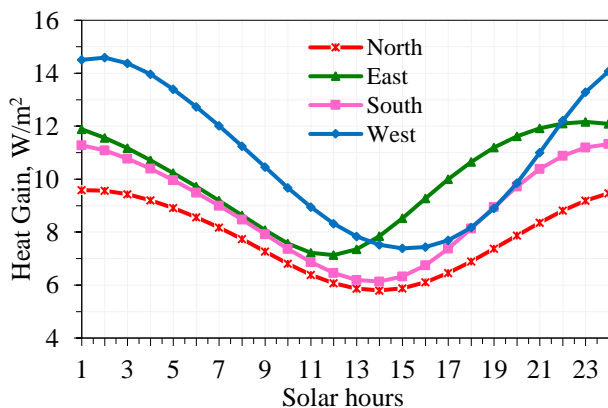

Figure 5. Heat gain values depend on the East, West, North, and South directions of the EPC50 wall

Figure 6 shows the hourly heat gain values of walls with different colors facing the South direction. Black, green, brown, and white colored surfaces have the highest and lowest heat gain values, respectively. The solar absorptance of the wall has a great influence on the heat gain values that the dark surfaces absorb more solar radiation. As a result, constructing buildings in white or near-white colors in regions with high outdoor temperatures and solar radiation intensity will reduce cooling expenditures.
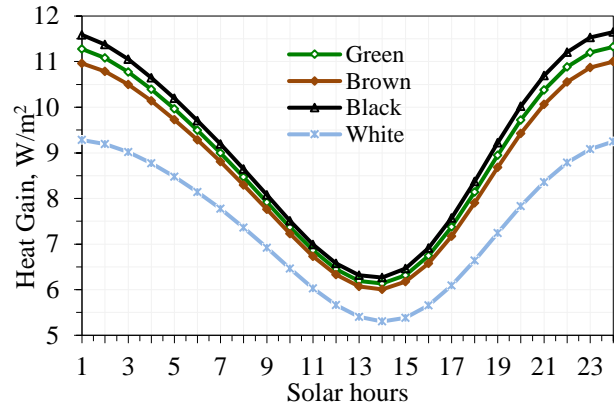

Figure 6. Hourly heat gain values of south-facing walls with different colors.

Hourly heat gain variations of green-colored NC and EPC walls/roofs with different expanded perlite ratios due to the South direction are shown in Figures 7 and 8, respectively. It was observed that the highest heat gain occurs for the wall and roofs constructed with NC and followed by EPC10, EPC20, EPC30, EPC40, EPC50, and EPC60, respectively. When the maximum heat gain values for the walls in 24 hours are compared; the highest heat gain value was calculated as 65.909 W/m² for NC and the lowest heat gain value was calculated as 32.724 W/m² for EPC60. While these values for roofs are 151.454 W/m² for NC, it is 78.668 W/m² for EPC60. An R1-type roof is widely used in Turkey, especially in old buildings. Since this roof type consists of only 2 cm plaster and 12 cm concrete, it is understood that it is highly affected by the outdoor temperature and solar radiation, and the hourly heat gain amplitude is very high for both light and dark colors. The value of 151.454 W/m² obtained for NC indicates that since the capacity of the cooling unit to be used for an R1-type roof dwelling must be very high, it will bring worse living conditions, a higher investment, and operating cost. As a result, an R1-type roof should not be preferred in residences.
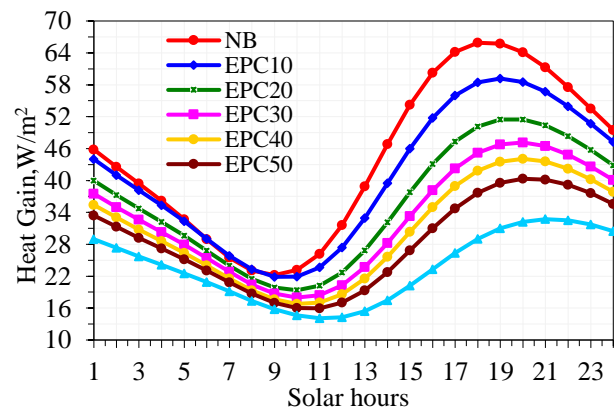

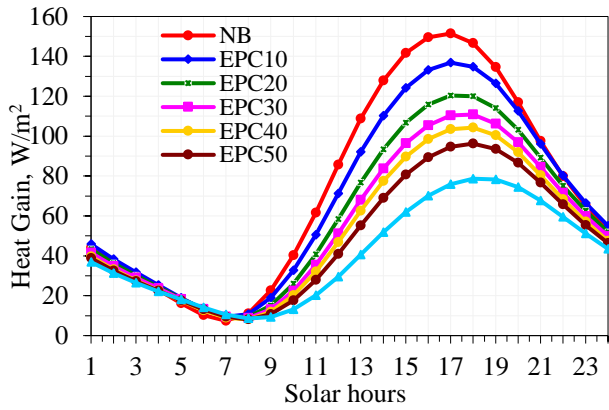**Figure 7.** Daily variation of heat gain values of NC and EPC walls facing south

Figure 8. Daily **v**ariation of heat gain values of NC and EPC flat roofs

Hourly variations of heat gain values of NC and PC walls and flat roofs with different pumice aggregate ratios due to the South direction are shown in Figures 9 and 10, respectively. It was observed that the wall and roof constructed with NC material had the highest heat gain values, followed by PC20, PC40, PC50, PC60, PC80, and P100, respectively. When the maximum heat gain values for the walls in 24 hours are compared; the highest heat gain value was calculated as 65.909 W/m^2 for NC and the lowest heat gain value was calculated as 24.09 W/m^2 for PC100. While these values for the roof were 151.454 W/m^2 for NC, and 58.319 W/m^2 for PC100.
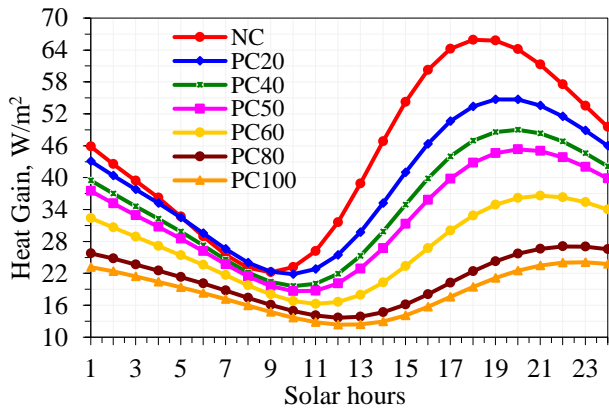

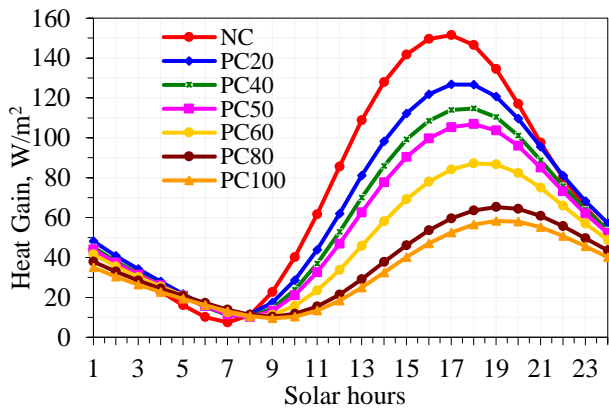**Figure 9.** Daily variation of heat gain values of NC and PC walls facing south

Figure 10. Daily **v**ariation of heat gain values of NC and PC flat roofs

Hourly heat gain variations of NC and RC walls and flat roofs with different waste rubber aggregate ratios due to the South direction are shown in Figures 11 and 12, respectively. It was observed that the wall and roof constructed with NC material had the highest heat gain values, followed by RC10, RC20, RC30, RC40, RC50, and RC60, respectively. When the maximum heat gain values for the walls in 24 hours are compared; the highest heat gain value was calculated as 65.909 W/m^2 for NC and the lowest heat gain value was calculated as 32.558 W/m^2 for RC60. While these values for the roof were 151.454 W/m^2 for NC, it was 77.85 W/m^2 for RC60.
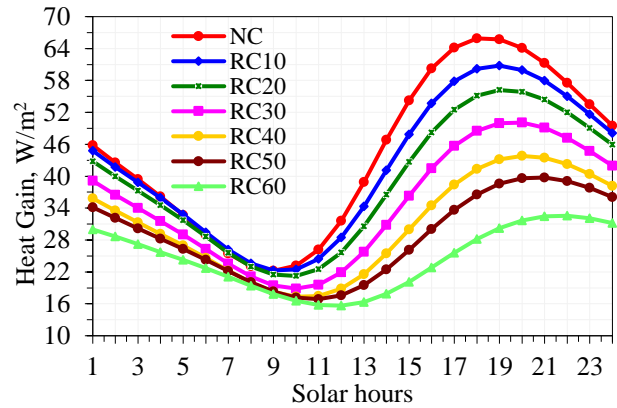

Figure 11. Daily **v**ariation of heat gain values of NC and RC walls facing south
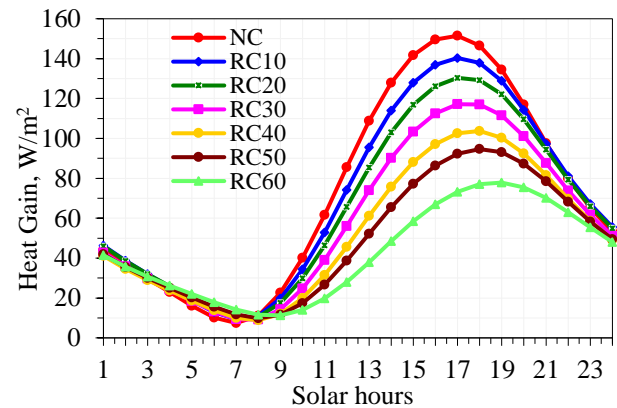

Figure 12. Daily **v**ariation of heat gain values of NC and RC flat roofs

The hourly heat gain values obtained by using some building materials on the roof and south-facing walls are indicated in Figure 13 and Figure 14, respectively. It can be shown that walls and roofs made of NC, which have the maximum thermal conductivity and thermal diffusivity, have the greatest heat gain. The thermal conductivity and diffusivity of the materials have been found to significantly affect the thermal performance of the constructions. A heat gain of 11,324 W/m^2 for the walls and 28,194 W/m^2 for the roof was obtained for the walls constructed with PC40-EPC60, which has the lowest thermal conductivity and thermal diffusivity values. As can be seen here, the heat gain of the PC40-EPC60 wall is approximately 1/6 of the NC wall. High heat gain is undesirable in terms of both comfort and high cooling load. Consequently, with a high cooling load, the capacity of a cooling system, the initial investment, and the operating cost will increase.
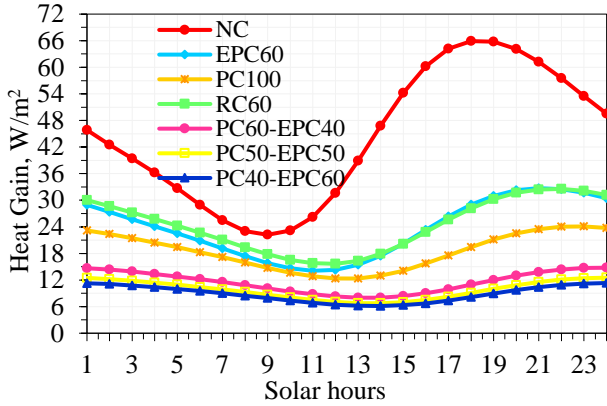
Figure 13. Daily **v**ariation of heat gain values of different wall constructions due to south
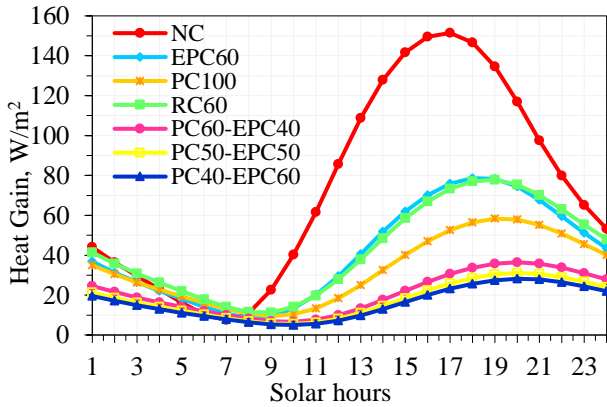

Figure 14. Daily **v**ariation of heat gain values of different roof constructions

Briquette, blockbims, curtain concrete, aerated concrete, and brick are generally used as wall materials in Turkey. Figure 14 shows the comparison of the highest heat gain values of the commonly used in our country according to their thickness in a design day due to the South direction. The highest heat gain in a day for a building construction occurs at different hours depending on the thermophysical properties and heat storage capabilities of the wall material. For each wall material, the heat gain decreases as the wall thickness and, accordingly, the thermal resistance increase. This figure explains which wall thickness for NC-constructed walls corresponds to brick, block, briquette, aerated concrete, PC40-EPC60 walls, or to each other. By the way, it is shown how much wall heat gain is necessary for a wall thickness and each of the structures. As can be seen from the figure, the highest heat gain for the NC wall with a thickness of 20 cm will be equal to the same heat gain with briquettes and bricks of 12.91 cm and 10.72 cm thickness, respectively. However, it is seen that the highest heat gain for the 10 cm thick PC40-EPC60 wall corresponds to 29.75 cm brick, 15.43 cm blockbims, and 11.8 cm aerated concrete. The heat gains of aerated concrete and PC40-EPC60 walls are generally close to each other. Although by using PC40-EPC60 as wall material, which is easily produced from domestic sources and cheaper than aerated concrete having disadvantages such as high production costs and lack of plaster

adhesion, is important in reducing energy consumption due to heating and cooling, as well as operating and initial costs for low-carbon buildings. The results also reveal that, especially in massive buildings, the thicker element would absorb heat and delay the time when conditions would become uncomfortable. Although the obtained result is consistent well with Refs. (Jin et al., 2012; Barrios et al., 2011) the thickness of the wall material is not particularly deterministic in terms of heat gain due to limits of practical applications in residential buildings.
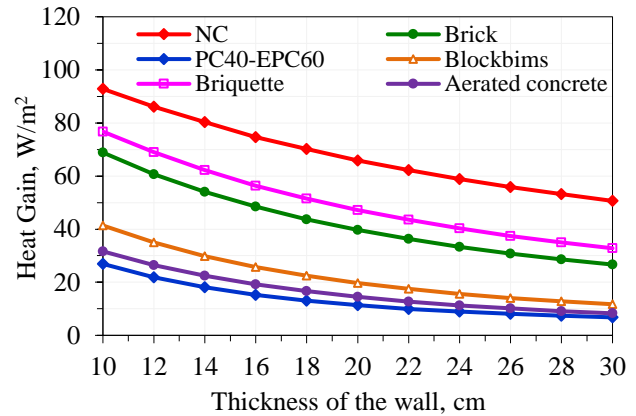

Figure 15. Comparison of the highest heat gain values of commonly used wall materials with different thicknesses

5. Conclusions

In this study, experimental and theoretical investigations were carried out to determine the best thermal performance wall or roof types for low-carbon buildings. The followings conclusions obtained from the study can be drawn:

1. The results indicated that the highest heat gain values in a design day for flat roofs and walls are obtained; respectively, as follows; 151.454 W/m² and 65.909 W/m² for NC, 78.668 W/m² and 32.724 W/m² for EPC60, 58.319 W/m² and 24.09 W/m² for PC100 and 77.85 W/m² and 32.558 W/m² for RC.

2. When the wall materials commonly used in Turkey are compared, it is seen that the highest heat gain in the 10 cm thick PC40-EPC60 wall corresponds to 29.75 cm brick, 15.43 cm blockbims, and 11.8 cm aerated concrete.

3. The improvement of heat gain values is greatly influenced by the thermal characteristics of the wall or roof materials. Thermal diffusivity and conductivity are two crucial properties in particular, and materials with low thermal conductivity have small heat gain amplitude values.

4. In all types of roofs and walls, the lowest heat gain value was obtained for the PC40-EPC60, but the highest ones were obtained for the NC.

Consequently, using construction types with high thermal insulation characteristics in the buildings provides energy efficiency and contributes directly to the economy of our country.

Nomenclature

c	specific heat (kJ/kg K)
h_i	heat transfer coefficient at inner surface (W/m² K)
h_o	heat transfer coefficient at outer surface (W/m² K)
i,j	complex arguments
I_T	radiation flux on tilted surface (W/m²)
I_{bT}	beam radiation flux on tilted surface (W/m²)
I_{dT}	diffuse radiation flux on tilted surface (W/m²)
I_{rT}	reflected radiation flux on horizontal surface (W/m²)
λ	thermal conductivity (W/m K)
L	thickness (m)
p	time period (h)
t	time (s)
T_a	ambient air temperature (°C)
T_e	sol-air temperature (°C)
T_r	room temperature (°C)

Greek symbols

α	thermal diffusivity (m²/s)
$α_s$	absorptance of surface
ρ	density (kg/m³)
$ω_j$	complex frequency
δ	declination
ε	emissivity of a surface
ΔR	difference between long-wave radiation incident on the surface from the sky (W/m²)
τ, $τ_n$, $τ_{np}$	dimensionless time terms
$ρ_g$	ground reflectance
ω	hour angle
φ	latitude angle
γ	surface azimuth angle

Subscripts

i	inside
o	outside
N	number of layers

References

ACI Committee 122. 2002. Guide to thermal properties of concrete and masonry systems. American Concrete Institute.

Argunhan, Zeki. 2017. Yapı Elemanlarında Kullanılan Atık Lastiklerin Isıl Performansının İncelenmesi. Dicle Üniversitesi Mühendislik Fakültesi Mühendislik Dergisi 8(3):621–30.

Bansal, Karan, Souma Chowdhury, and M. Ram Gopal. 2008. Development of CLTD Values for Buildings Located in Kolkata, India. Applied Thermal Engineering 28(10):1127–37. doi: 10.1016/j.applthermaleng.2007.08.005.

Barrios, G., G. Huelsz, R. Rechtman, and J. Rojas. 2011. Wall/Roof Thermal Performance Differences between Air-Conditioned and Non Air-Conditioned Rooms. Energy and Buildings 43(1):219–23. doi: 10.1016/j.enbuild.2010.09.015.

Bouguerra, A., A. Ledhem, F. Barquin, R. M. Dheilly, and M. Queneudec. 1998. Effect of Microstructure on the Mechanical and Thermal. Cement and Concrete Research 28(8):1179–90.

Chandra, Satish, and Berntsson, Leif. 2002. Applications of Lightweight Aggregate Concrete. Lightweight Aggregate Concrete Science, Technology, and Applications. New York: William Andrew Inc, 369-400.

De Rosa, Mattia, Vincenzo Bianco, Federico Scarpa, and Luca A. Tagliafico. 2016. Impact of Wall Discretization on the Modeling of Heating/Cooling Energy Consumption of Residential Buildings. Energy Efficiency 9(1):95–108. doi: 10.1007/s12053-015-9351-5.

Demirboğa, Ramazan, and Rüstem Gül. 2003. The Effects of Expanded Perlite Aggregate, Silica Fume and Fly Ash on the Thermal Conductivity of Lightweight Concrete. Cement and Concrete Research 33(5):723–27. doi: 10.1016/S0008-8846(02)01032-3.

Duffie, John A., and Beckman, William A. 1980. Solar engineering of thermal proces. Wiley, New York.

Erdal, Gülistan, Hilmi Erdal, and Kemal Esengün. 2008. The Causality between Energy Consumption and Economic Growth in Turkey. Energy Policy 36(10):3838–42. doi: 10.1016/j.enpol.2008.07.012.

Hahn, David, and Özişik, Necati. 2012. Heat conduction. John Wiley & Sons.

Handbook, ASHRAE 1993. ASHRAE Fundamentals. Atlanta. New York, NY, USA, 27-27.

Jin, Xing, Xiaosong Zhang, Yiran Cao, and Geng Wang. 2012. Thermal Performance Evaluation of the Wall Using Heat Flux Time Lag and Decrement Factor. Energy and Buildings 47:369–74. doi: 10.1016/j.enbuild.2011.12.010.

Naji, Sareh, Shahaboddin Shamshirband, Hamed Basser, U. Johnson Alengaram, Mohd Zamin Jumaat, and Mohsen Amirmojahedi. 2019. Retraction Note: Soft Computing Methodologies for Estimation of Energy Consumption in Buildings with Different Envelope Parameters (Energy Efficiency, (2016), 9, 2, (435-453), 10.1007/S12053-015-9373-Z). Energy Efficiency 12(3):827. doi: 10.1007/s12053-018-9761-2.

Oktay, Hasan, Recep Yumrutaş, and Abdullah Akpolat. 2015. Mechanical and Thermophysical Properties of Lightweight Aggregate Concretes. Construction and Building Materials 96:217–25. doi: 10.1016/j.conbuildmat.2015.08.015.

Oktay, Hasan, Recep Yumrutas, and Zeki Argunhan. 2020. An Experimental Investigation of the Effect of Thermophysical Properties on Time Lag and Decrement Factor for Building Elements. Gazi University Journal of Science 33(2):492–508. doi: 10.35378/gujs.615322.

Ozbalta, Türkan Goksal, and Necdet Ozbalta. 2010. The Effects of Insulation Location and Thermo-Physical Properties of Various External Wall Materials on Decrement Factor and Time Lag. Scientific Research and Essays 5(23):3646–59.

Real, Sofia, Cinthia Maia, Jos Alexandre Bogas, and Maria Da Glaria Gomes. 2021. Thermal Conductivity Modelling of

Structural Lightweight Aggregate Concrete. Magazine of Concrete Research 73(15):798–809. doi: 10.1680/jmacr.19.00320.

Think harder concrete. Cement Association of Canada. www.cement.ca/en/Think-harder-Concrete.html; 2013.

TMMOB. 2005. Yalıtım Kitabı Yayın No: MMO/2005/399. TMMOB Makina Mühendisleri Odası, İstanbul Şubesi Kütüphanesi, İstanbul.

Ulgen, Koray. 2002. Experimental and Theoretical Investigation of Effects of Wall's Thermophysical Properties on Time Lag and Decrement Factor. Energy and Buildings 34(3):273–78. doi: 10.1016/S0378-7788(01)00087-1.

Uysal, Habib, Ramazan Demirboga, Remzi Şahin, and R. Gül. 2004. The Effects of Different Cement Dosages, Slumps, and Pumice Aggregate Ratios on the Thermal Conductivity and Density of Concrete. Cement and Concrete Research 34(5):845–48. doi: 10.1016/j.cemconres.2003.09.018.

Vaou, V., and D. Panias. 2010. Thermal Insulating Foamy Geopolymers from Perlite. Minerals Engineering 23(14):1146–51. doi: 10.1016/j.mineng.2010.07.015.

Yumrutaş, Recep, Önder Kaşka, and Erdal Yildirim. 2007. Estimation of Total Equivalent Temperature Difference Values for Multilayer Walls and Flat Roofs by Using Periodic Solution. Building and Environment 42(5):1878–85. doi: 10.1016/j.buildenv.2006.02.020.

Assessment of architectural heritage characteristics and seismic behavior of Ziyaeddin Han Tomb

Fatih Avcil [a,*] (iD) , Enes Arkan [a] (iD)

[a] Bitlis Eren University, Department of Civil Engineering, TR-13000, Bitlis, Turkey

ARTICLE INFO

ABSTRACT

Historical structures built by different civilizations that have survived to the present day have an important place within the scope of the protection of cultural heritage. Bitlis province, where many different civilizations lived and located in a strategic position on the Silk Road, contains many different types of historical structures. Within the scope of this study, the Ziyaeddin Han Tomb, which was built in masonry during the Şerefhans under the rule of the Ottoman period, has been taken into account. Besides, the architectural features of the tomb, detailed information are given about the current structural situation. As a consequence of on-site measurements, a numerical model of the historical tomb was formed using the finite element method (FEM) and structural analyzes were enforced. Structural analyzes were performed for the tomb, in which the macro modeling technique was applied, considering four different earthquake ground motion levels, 2%, 10%, 50%, and 68%, with a probability of exceedance in 50 years. Besides, the time history analysis was applied to take advantage of the acceleration record of an earthquake that occurred in the near region and the recent history of this tomb located in the city center of Bitlis. The structural performance of the tomb was tried to be determined by using the displacement and drift ratio obtained.

1. Introduction

In our country, which has many historical and cultural structures, preserving these structures and transferring them to the next generations is one of the most important research topics of today. Historical buildings are an important indicator of people's economic status, engineering-architecture accumulation, and belief styles at the time they were built. The protection of these precious structures is a common problem of humanity and there are many studies on this subject (Karaşin et al. 2016a; Hadzima-Nyarko et al. 2018; Gunes et al. 2021; Karalar and Cavusli 2020; İzol et al. 2022a). As the studies cover different fields of specialization, they are often studied in engineering, architecture, art history, etc. interdisciplinary studies of fields of science may be required.

(Giordano et al. 2002; Işık et al. 2019; Özodabaş and Artan 2021; Milani et al. 2018; Bilgin and Ramadani 2021; Akan et al. 2021; Berto et al. 2022).

In the province of Bitlis, which is strategically located in the Vangölü basin and on the Silk road, there are many historical buildings built by many different civilizations due to being a very old settlement. Among these structures, mosques, minarets, bridges, baths, and tombs are prominent and there are limited studies in the literature about these structures (Oğuz and Aksulu 2016; Işık et al. 2018; Işık et al. 2019b). This study can also be regarded as a case study to determine the architectural features of historical buildings, to model and strengthen them with the finite element method, to determine the material characteristic used, and to determine their seismic behavior using different seismic analysis methods. On the other hand, Karasin et al. (2016b) made structural analyzes of

* *Corresponding author.* Tel.: +90 0434 222 00 00 (3619) fax: + +90 434 222 91 45
  E-mail address: favcil@beu.edu.tr
  ORCID : *0000-0001-6550-550X (F. Avcil), 0000-0002-6588-7234 (E. Arkan)*

the Ulu Mosque based on observation. Structural analyzes were carried out by Işık et al. (2022a) for all of the Five Minarets, the significant historical buildings of Bitlis, and the subject of songs. In the study by Işık et al. (2022b), the exhaustive structural and architectural analyzes of the Ziyaeddin Han Tomb were performed considering the different probabilities of exceedance according to the current earthquake code used in Turkey.

In the context of this investigation, structural analyzes were performed for the masonry Ziyaeddin Han Tomb, located in the city center of Bitlis, in terms of both architecture and engineering. Tombs are generally built with a cylindrical or polygonal body, covered with a dome from the inside and a conical or pyramidal roof from the outside. The purpose of choosing this tomb is that it differs architecturally and structurally (Doğru et al. 2017). This tomb, which has a very rigid structure, has walls that start with a square prism-shaped lower section from the outside, end with a dodecagonal plan at the top, and has a flat roof cover. Current earthquake regulations were used in structural analysis. Literature was used for the properties of Ahlat stone as given below used in the construction of the tomb, and a FEM of the tomb was formed by using the macro modeling method with on-site measurements. First of all, modal analysis was performed, stresses were calculated for four different earthquake ground motion levels, and finally, displacements in the historical tomb under the effect of the 2011 Van earthquake that occurred in the near region and the recent history were found.

2. Material and Methods

2.1. Ziyaeddin Han Tomb

Located in the city center of Bitlis, the Ziyaeddin Han tomb is in the complex built around the İhlasiye (Gökmeydan) Madrasa. This complex was registered by the Diyarbakır Cultural and Natural Heritage Preservation Board in 1989 together with the tomb in question. Projects for the restoration of these structures, except Şemsiye Masjid, were drawn in 1997 and then restored by the Ministry of Culture and Tourism (Url1, VKVKBKM. 2022). In addition to the madrasah in the complex; There are four tombs-cupolas and a mosque. The tomb was built in front of the gate of the madrasah opening to the south. The architectural layout plan of the complex is shown in Figure 1.

It is stated in various sources that the building, which does not have an inscription, belongs to Emir Ziyaeddin Han, who died in 1390 or 1394, and was built at that time (Arık, 1971; Erkan, 1977; Uluçam, 2002). As shown in Figure 2, one of the broken tombstones inside the tomb belongs to Emir Ziyaeddin and has the date 1621-1622 (1031 H). Looking at the genealogy of the Şerefhans Principality, which ruled in Bitlis, it is known that the 6th Ruler Emir Ziyaeddin was the administrator until 1390, and the 21st ruler Ziyaeddin Han was the administrator between 1655 to 1656 (Vilayetlerimizin Tarihi, 1968). The date indicated on the tombstones corresponds to the period of the 19th ruler Şemseddin IV (1597-1638).

Figure 1. Ziyaeddin Han tomb layout plan.

الدنيا ساعه فاجعلها طاعه
هذه؟ روضة السعيد الشهيد
المغفور المرحوم الامير الكبير
شرف؟ الامر الكبير ضياءالدين
خان
فى سنه ١٠٣١

- Ed-dünya sa'eh, fec'aelaha ta'eh
- Hâzâ ravdet'üssaid eşşehîd
- El mağfur, Errahîm, el emîr el Kebir şeref
- El emrel kebir Ziyaeddin Han
- Fî seneh 1031

Figure 2. The broken tombstone in the Ziyaeddin Han Tomb and its transcription (by Abdulhakim ARKAN)

The tomb consists of a burial section in which there are six cist graves. Arık (1971) states that the tomb was built without a prayer hall or this part was destroyed later. Its walls, which start with a square prism-shaped lower section from the outside, end with a dodecagonal plan at the top. When transiting to this plan, the corners were chamfered from the outside, as shown in Figure 3.

The lower part of the interior is also square in shape, just like the exterior. The vault was built after the 90 cm straight wall in the interior. As shown in Figure 4, the interior space forming the mirror vault supports 2 arches coming from each side.

Figure 3. Exterior view of Ziyaeddin Han Tomb

Figure 4. Interior view and mirror vault of Ziyaeddin Han Tomb

The tomb remained under the ground up to the upper level of the entrance gate in the northern part. The entrance is reached by a five-step staircase. On each of the side facades, there are two windows, one of which is mostly under the ground, and the other is on the upper level. As shown in Figure 5(a), Tuncer's (1991) drawing shows decorations on the upper side and sides of the door; there is no decoration on the door in its current situation shown in Figure 5(b). The decoration on the entrance door was probably destroyed and was not replaced during the restoration. Today, there are decorations only on the lower side parts of the entrance door. There is a passionflower motif as shown in Figure 5(c) above the lower window in the south.

Arık (1967, 1971) evaluated it in the typology of a tomb with a polygonal prism-shaped drum and a pointed cone on a cubic body. However; It is considered a unique building type due to both its incomplete/destroyed superstructure and the interior structure with arch mirror vaults.
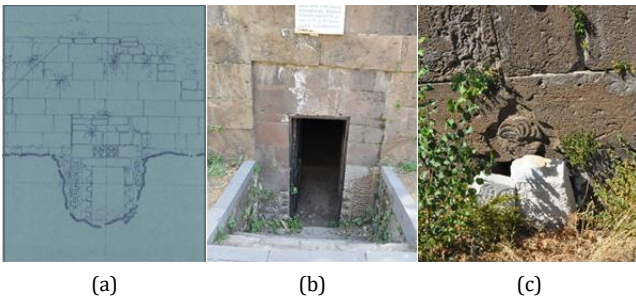

(a)   (b)   (c)

Figure 5. Ziyaeddin Han Tomb (a) 1991 drawing by Tuncer (b) Decoration around the tomb entrance (c) passionflower motif on the window

In order to model the Ziyaeddin Han tomb, on-site measurements were made, and the plan and section were drawn to scale as seen in Figure 6. The tomb sits on a base of 8.99 x 8.99 meters from the outside and is 3.55 meters above the ground. The entrance gate is located below 1.23 meters of ground level. Its height from the interior floor to the mirrored vault is 4.26 meters.
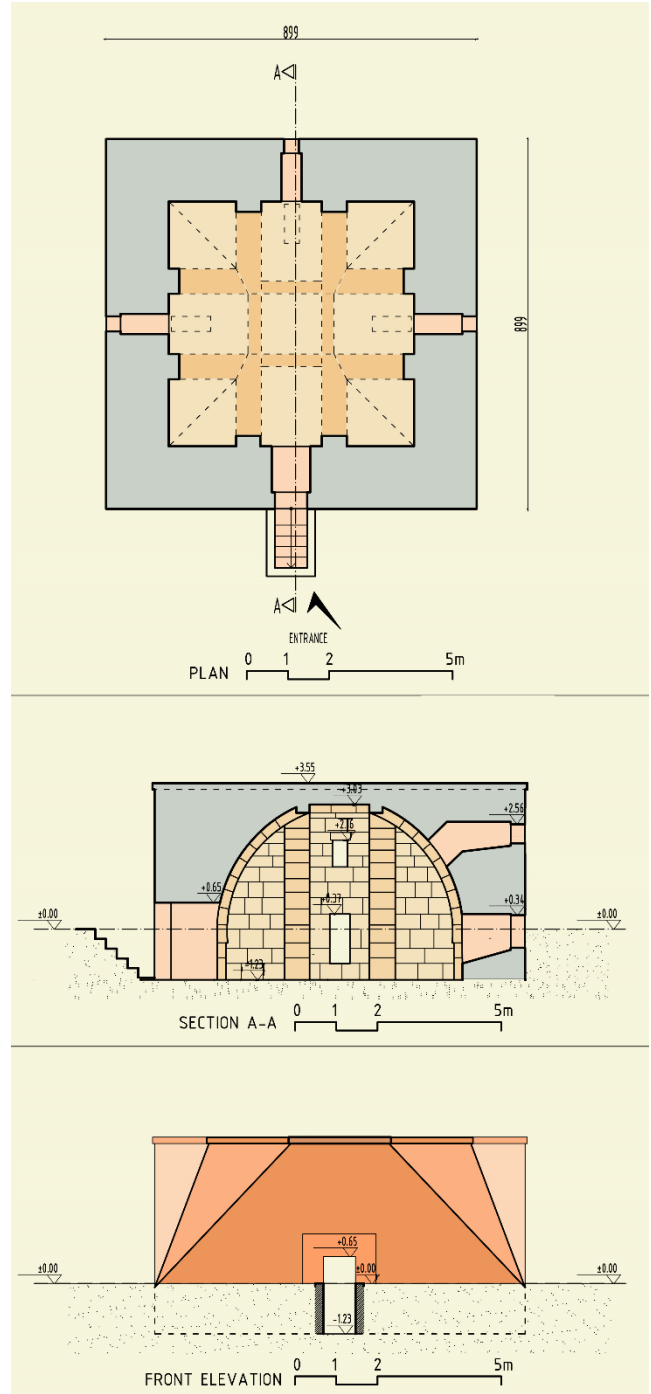

Figure 6. Plan, section, and view of Ziyaeddin Han Tomb

3. Results and Discussion

For the location of the dome, the local soil class ZB was taken into account in the structural analysis. The characteristics of this local soil class, which are determined in the soil survey reports given in the Turkish Building Earthquake Code (TBEC -2018), which are the subject of the study and made by the relevant public institutions, are shown in Table 1.

Table 1. Local soil class type ZB (TBEC-2018)

Local Soil Class	Soil Type	Upper average at 30 meters		
		(VS)30 [m/s]	(cu)30 [kPa]	(N60)30 [pulse/30cm]
ZB	Less weathered, reasonably strong rocks	760-1500	----	----

The vertical and horizontal design spectrum attained from the Turkish Earthquake Hazard Map Interactive Web Earthquake Application (AFAD, 2022) and utilized in structural analysis for the studied tomb is shown in Figure 7.
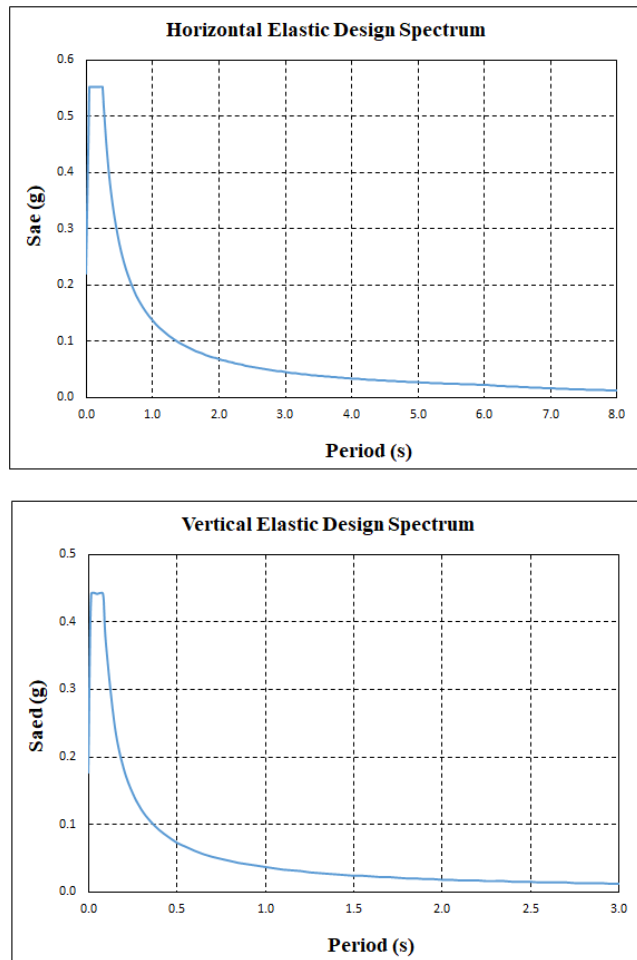

Figure 7. Vertical and horizontal elastic design spectrums

The sources in the literature were used for the material properties of the Ahlat stone used in the historical tomb. The unit volume weight (γ), modulus of elasticities (E), and the Poisson ratio (n) are taken as a constant in structural modeling. The structural parameters of Ahlat stone are given in Table 2.

Table 2. Material properties of Ahlat stone (Isik et al. 2018; Özvan et al. 2015)

	Unit Volume Weight γ (kN/m3)	Modulus of Elasticity, E (MPa)	Poisson ratio, n
Ahlat	24.5	5000	0.2

To do a comparison assessment, the local soil class ZB in the Turkish Building Earthquake Code that was established in the site-survey reports finished by the relevant public facilities for the location of the Ziyaeddin Han Tomb was taken into account. There are four distinct earthquake ground motion levels identified in TBDY 2018. The first one is the "largest earthquake ground motion level" (DD-1), with a spectral magnitude of 2% probability of exceedance in 50 years. The second is the "standard design earthquake ground motion level" (DD-2) with a spectral magnitude of 10% probability of exceedance in 50 years. The third is the "frequent earthquake ground motion level" (DD-3) with a spectral magnitude of 50% probability of exceedance in 50 years. The last is the "service earthquake ground motion level" (DD-4), with a spectral magnitude of 68% probability of exceedance in 50 years. The peak ground velocities (PGV) and the peak ground accelerations (PGA) were determined for the different probability of exceedance for the selected settlement as given in Table 3.

Table 3. PGV and PGA of the tomb for different ground motion levels

City	Peak ground velocity (cm/s)-PGV Earthquake ground motion level				Peak ground acceleration (g)-PGA Earthquake ground motion level			
	DD-1	DD-2	DD-3	DD-4	DD-1	DD-2	DD-3	DD-4
Bitlis	28.215	15.081	6.508	4.847	0.490	0.260	0.106	0.077

Updates have been made to several computer applications that help with data transfer and deliver integrated outcomes to application projects for computing and designing today's current engineering structures. Masonry constructions have different structural systems than current engineering structures. For the structural analysis of such structures, finite element analysis is chosen. The creation of a numerical model of the structure under examination is the first stage in this procedure. Numerical modeling is the mathematical representation of structural system components made up of various materials and having different cross-section geometries. Masonry structure numerical modeling using the finite element approach calls for a lot of processing capability (Pande et al. 1989; İzol et al. 2022b; Pekgökgöz et al. 2022).

Structural analyzes for the tomb examined in the study were performed using the ABAQUS software (ABAQUS, 2011). The finite element model and the meshed structure model of the finite element model obtained in the software program are shown in Figure 8. While creating the structure, the vault, top beams, and wall were drawn separately and modeled as one part. In the finite element model of the tomb, the total number of nodes is 125353 and the total number of elements is 85958.

Quadratic tetrahedral elements (C3D10) were selected as the mesh type for the tomb.
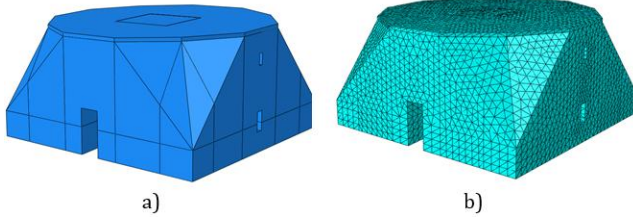

Figure 8. a) FEM of the tomb, b) Meshed model of the building

A modal analysis was first accomplished to ascertain the tomb's dynamic characteristics. The first ten modes that emerged in the building were taken into account when doing the modal analysis. Table 4 displays the effective modes' frequencies, natural vibration periods, and mass participation rates, in accordance with the model's modal analysis findings.

Table 4. Modal analysis results of the tomb model

Mode	Frequency (Hz)	Period (s)	Mass Participation Ratio (X) (%)	Mass Participation Ratio (Y) (%)	Total Mass Participation Ratio (X) (%)	Total Mass Participation Ratio (Y) (%)
1	23.426	0.043	0	0.77491	0	0.77491
2	23.837	0.042	0.77126	0	0.77126	0.77492
3	34.241	0.029	0	0.00197	0.77126	0.77689
4	41.775	0.024	0.0001	0	0.77136	0.77689
5	42.636	0.023	0	0.00034	0.77136	0.77723
6	43.462	0.023	0.00004	0	0.77139	0.77723
7	51.623	0.019	0.00004	0	0.77143	0.77723
8	52.746	0.019	0	0	0.77143	0.77723
9	55.564	0.018	0.00003	0	0.77146	0.77723
10	60.668	0.016	0.00137	0.77491	0.77283	0.77723

Analysis was performed in the ABAQUS software program (ABAQUS, 2011) for the Ziyaeddin Han tomb, considering the first five modes in which torsion occurs. The resulting mode shapes are shown in Figure 9.
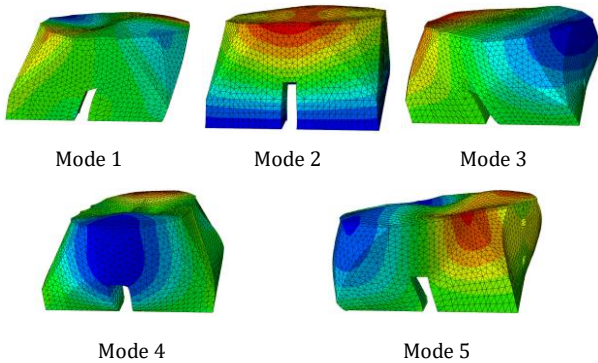

Figure 9. The first five modes of the tomb

The stress distributions obtained for earthquake ground motion levels DD-1, DD-2, DD-3, and DD-4 are shown in Figure 10 (a), (b), (c), and (d) respectively.
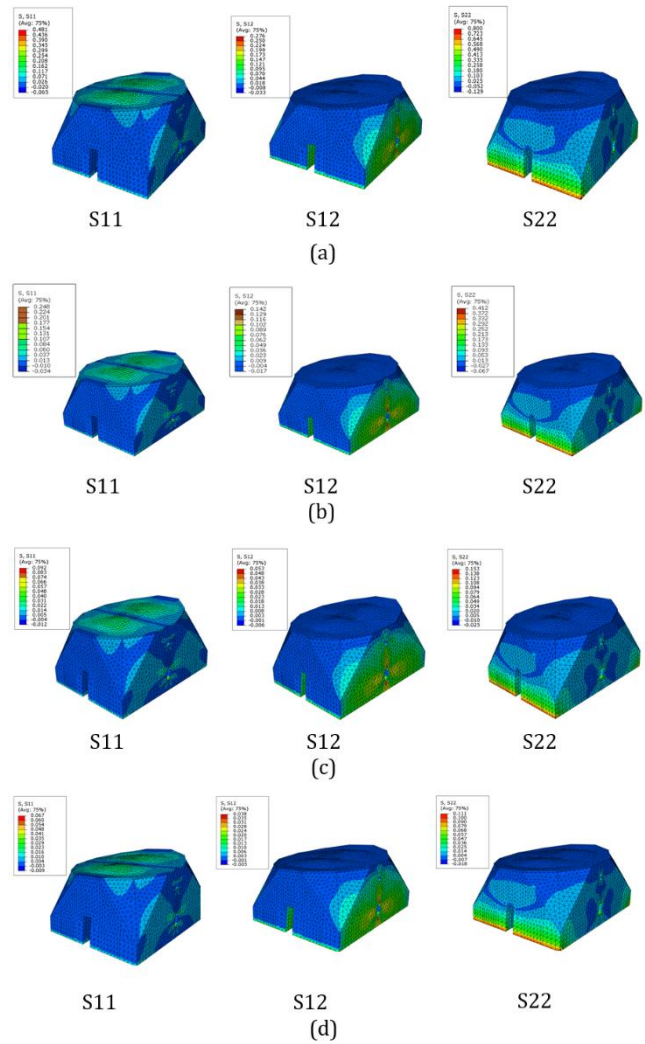

Figure 10. Stress distribution according to ground motion levels (a) DD-1, (b) DD-2, (c) DD-3, and (d) DD-4

The maximum base shear forces, displacements, and stresses obtained for different earthquake ground motion levels are shown in Table 5.

Table 5. The maximum base shear forces, displacements, and stresses found for the various earthquake ground motion levels

Ground Motion Level	Base Shear Force (N)	Displacement (mm)	S11 (MPa)	S12 (MPa)	S22 (MPa)
Bitlis DD-1	5.087×10^6	0.702	0.481	0.276	0.800
Bitlis DD-2	2.619×10^6	0.361	0.248	0.142	0.412
Bitlis DD-3	0.971×10^6	0.134	0.092	0.053	0.153
Bitlis DD-4	0.705×10^6	0.097	0.067	0.038	0.111

The displacements obtained during the study were used to determine performance levels. Limit value hypotheses from the Turkey Earthquake Risk Management Guide for Historic Buildings (TERMFHB-2017) were applied for this purpose. The use of linear computation for the "immediate occupancy" (IO)

performance level and either linear or non-linear computation techniques for the "life safety" (LS) and "collapse prevention" (CP) performance levels were considered to be sufficient. Figure 11 shows the minimum limits that must be provided if one of these computation techniques is chosen.
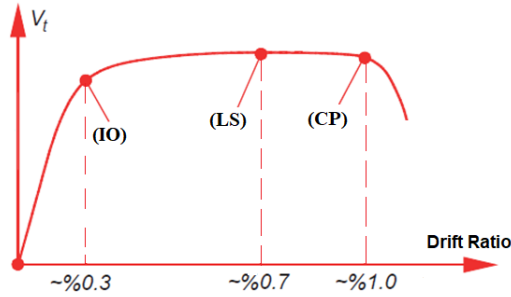

Figure 11. Limit states and pushover curve (from TERMFHB-2017)

In this section of the paper, a time history analysis will be performed under a selected acceleration record. Acceleration records of the Van (located in eastern Turkey) earthquake, which is in the closest region to Tomb and occurred in 2011, will be used. Figure 12 shows the Van South-North acceleration-time curve utilized in the analysis for this earthquake. Figure 13 displays the displacement-time graph that was produced as a consequence of the time history analysis.
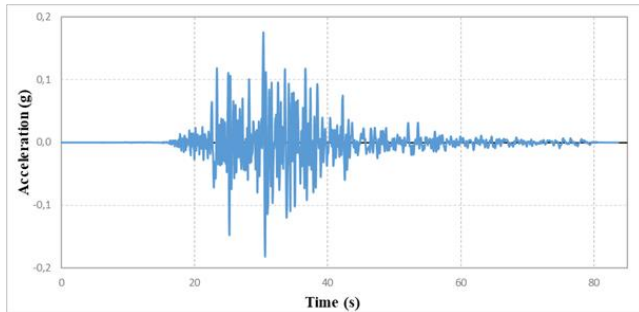

Figure 12. South–north acceleration–time graph of Van earthquake (2011)
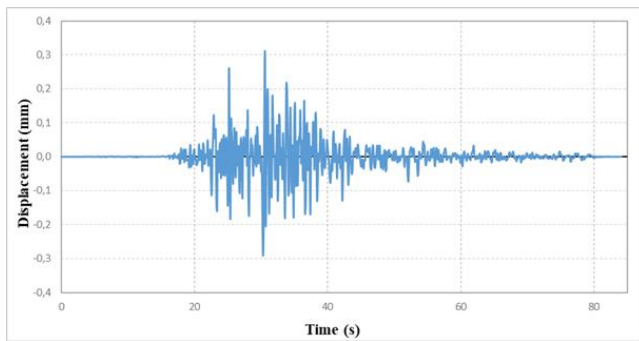

Figure 13. Time-history analysis (Van Earthquake) (Max=0.3 mm)

As a result of the 2011 Van earthquake acceleration recording, Ziyaeddin Han Tomb, whose time history analysis was performed and modeled with the finite element method, a displacement of 0.3 mm was obtained from the top of the structure. The largest drift-ratio value was calculated as 0.006%. The performance levels created by considering the displacement and drift-ratio values are shown in Table 6.

Table 6. Time-history analysis results and the limit performance level check

Regulation	Max. Displacement (mm)	Max. Drift-Ratio (%)	IO<%0,3		LS<%0,7		CP< %1	
TBEC (2018)	0.3	0.006	14.34	✔	33.46	✔	47.8	✔

Considering the largest displacement rate under the 2011 Van earthquake acceleration records used in the analysis, no damage is expected in the historical structure.

4. Conclusions

In this study, the Ziyaeddin Han Tomb, which is different from other tomb structures with its architectural and structural characteristics in the Turkish-Islamic period monumental tomb architecture, located in the city center of Bitlis, was examined. This structure, which started as a square type at the base and ended with a dodecagonal flat plan at the top, was built with Ahlat stone, its interior was created with a mirrored vault and a total of eight arches, two on each side.

To define the dynamic properties of this building, which was informed about its historical and detailed architectural features, a building model was created by making on-site measurements and analyzed with the finite element method using the ABAQUS software program (ABAQUS, 2011). Mode shapes, frequencies, and periods were found as a result of the modal analysis of this quite rigid structure. The period of this building, which is not high and was built partially in the ground, turned out to be quite low as expected.

Structural analyzes were investigated for the historical tomb, where the macro-modeling technique was performed according to the TBEC 2018, by taking into account the various earthquake ground motion levels with 2%, 10%, 50%, and 68% probabilities of exceedance in 50 years. The earthquake effect that the structure is subjected to grows as the probability of exceedance decreases, and correspondingly, the displacements and stresses grow.

As a result of the analysis made by considering the 2011 Van earthquake acceleration records, since it is in the area close to this tomb in the city center of Bitlis, the maximum displacement was found to be considerably lower than the value stipulated in the regulation. It has been observed that as long as there are no material deteriorations or material losses that may occur in the structure, there will be no negativity related to the earthquake resistance of the structure. This demonstrates how advanced engineering expertise and understanding were at the time the dome was constructed.

References

Abaqus, G., 2011. Abaqus 6.11. Dassault Systemes Simulia Corporation, Providence, RI, USA.

Akan, A. E., Başok, G. Ç., Er, A., Örmecioğlu, H. T., Koçak, S. Z., Cosgun, T., Uzdil O., and Sayin, B., 2021. Seismic evaluation of a renovated wooden hypostyle structure: A case study on a mosque designed with the combination of Asian and Byzantine styles in the Seljuk era (14th century AD). Journal of Building Engineering, 43, 103112

Arık, M. O. 1967. Erken Devir Anadolu-Türk Mimarisinde Türbe Biçimleri. Anadolu, (11), 57-100.

Arık, M. O., 1971. Bitlis Yapılarında Selçuklu Rönesansı, Baskı No:1, Selçuklu Tarih ve Medeniyeti Enstitüsü.

Berto, L., Talledo, D. A., Bruschi, G., Zamboni, I., Lazzarini, E., Zofrea, C., Faccio, P., and Saetta, A. 2022. A Multidisciplinary Approach for the Vulnerability Assessment of a Venetian Historic Palace: High Water Phenomena and Climate Change Effects. Buildings, 12(4), 431.

Bilgin, H., and Ramadani, F., 2021. Numerical Study to Assess the Structural Behavior of the Bajrakli Mosque (Western Kosovo). Advances in Civil Engineering, 2021.

Doğru, M., Büyüksaraç, A., Aksoy, E., Karahan, R., Yakar, M., Ekinci, Y. L., Demirci A., ULVİ, A., and Toprak, A. S. 2017. Dünya Mirası Ahlat Selçuklu Mezarlığı İle Kümbetlerin Lidar Ve Jeofizik Yöntemlerle Araştırılması, Yüzey Ve Yüzeyaltı Yapı Modellemesi. Uluslararası Türkçe Edebiyat Kültür Eğitim (Teke) Dergisi, 6(1), 17-42.

Erkan, S., 1977. Türkiye'de Vakıf Abideler ve Eski Eserler-II; Vakıflar Genel Müdürlüğü Yayınları: Ankara

Giordano, A., Mele, E., De Luca, A., 2002. Modelling of historical masonry structures: comparison of different approaches through a case study. Engineering Structures; 24: 1057-1069.

Gunes, B., Cosgun, T., Sayin, B., Ceylan, O., Mangir, A., and Gumusdag, G., 2021. Seismic assessment of a reconstructed historic masonry structure: A case study on the ruins of Bigali castle mosque built in the early 1800s. Journal of Building Engineering, 39, 102240.

Hadzima-Nyarko, M., Ademovic, N., Pavic, G., and Sipos, T.K., 2018. Strengthening techniques for masonry structures of cultural heritage according to recent Croatian provisions. Earthquakes and Structures; 15: 473-485.

Işık, E., Antep, B., and Karaşin, İ. B., 2018. Structural Analysis of Ahlat Emir Bayındır Bridge. Bitlis Eren University Journal of Science and Technology, 8(1), 11-18.

Işık, E., Antep, B., Büyüksaraç, A., and Işık, M. F., 2019a. Observation of behavior of the Ahlat Gravestones (TURKEY) at seismic risk and their recognition by QR code. Structural Engineering and Mechanics, An Int'l Journal, 72(5), 643-652.

Işık, E., Antep, B., and Büyüksaraç, A., 2019b. Structural analysis and mapping of historical tombs in Ahlat District (Bitlis, Turkey). Electronic Journal of the Faculty of Civil Engineering Osijek-e-GFOS, 10(18), 22-35.

Işık, E., Harirchian, E., Arkan, E., Avcil, F., and Günay, M., 2022a. Structural analysis of five historical minarets in Bitlis (Turkey). Buildings, 12(2), 159.

Işık, E., Avcil, F., Harirchian, E., Arkan, E., Bilgin, H., and Özmen, H. B., 2022b. Architectural Characteristics and Seismic Vulnerability Assessment of a Historical Masonry Minaret under Different Seismic Risks and Probabilities of Exceedance. Buildings, 12(8), 1200.

İzol, R., Türkmen, O., Gürel, M. A., and Turgut, P., 2022a. Forms, and Vertical and Lateral Load Capacities of Columns in Mimar Sinan's Mosques. Bitlis Eren Üniversitesi Fen Bilimleri Dergisi, 11(2), 652-662.

İzol, R., Gürel, M. A., and Buyuktaskin, H. A. A., 2022b. Investigation of the effectiveness of nature-inspired buttress forms in supporting masonry structures. Građevinar, 74(07.), 573-586.

Karalar, M., and Cavusli, M., 2020. Tarihi Rombaki Yığma Yapısının Performans Değerlendirmesi. Bitlis Eren Üniversitesi Fen Bilimleri Dergisi, 9(1), 226-247.

Karasin, I. B., and Isık, E., 2016a. Protection of Ten-Eyed Bridge in Diyarbakır. Budownictwo i Architektura, 15(1), 87-94.

Karaşin, İ. B., Işık, E., and Eren, B., 2016b. Structural Analysis of Bitlis Grand Mosque. In International Conference on Natural Science and Engineering (ICNASE-2016), Kilis.

Milani, G., Valente, M., and Alessandri, C., 2018. The narthex of the Church of the Nativity in Bethlehem: a non-linear finite element approach to predict the structural damage. Computers & Structures, 207, 3-18.

Oğuz, G. P., & Aksulu, I. B., 2016. Geleneksel Bitlis evleri: koruma sorunları ve öneriler. Megaron, 11(1), 63-77.

Özodabaş, A., and Artan, C., 2021. Determination of Stress and Deformation Zones of Historical Mus Murat Bridge. Bilecik Şeyh Edebali Üniversitesi Fen Bilimleri Dergisi, 8(1), 413-429.

Özvan, A., Dinçer, İ., Akın, M., Oyan, V., and Tapan, M., 2015. Experimental studies on ignimbrite and the effect of lichens and capillarity on the deterioration of Seljuk Gravestones. Engineering geology, 185, 81-95.

Pande, G.N.; Liang, J.X.; Middleton, J., 1989. Equivalent elastic modul for unit masonry. Comput. Geotech. 8, 243–265.

Pekgökgöz, R., Avcil, F., Baltaci, G., and Gürel, M. A., 2022. Yığma İnşa Edilecek Bir Seyir Kulesinin Dinamik Analizi. Avrupa Bilim ve Teknoloji Dergisi, (35), 455-463.

TBEC, 2018. Turkish Building Earthquake Code; T.C. Resmi Gazete: Ankara, Turkey.

TERMFHB-2017, Tarihi Yapılar için Deprem Risklerinin Yönetimi Kılavuzu (TYDRYK), 2017. Vakıflar Genel Müdürlüğü, Ankara, Türkiye, 2017.

Tuncer, O.C., 1991. Anadolu Kümbetleri II, (Beylikler ve Osmanlı Dönemi), Ankara

Turkish Earthquake Hazard Map Interactive Web Application. Available online: https://tdth.afad.gov.tr (accessed on 1 November 2022).

Uluçam, A., 2002. Ortaçağ ve Sonrasında Van Gölü Çevresi Mimarlığı-II-Bitlis, Kültür Bakanlığı Yayınları, Ankara .

Url-1:https://bitlis.ktb.gov.tr/TR-56227/medreseler.html (29.11.2022, 15:13)

Vilayetlerimizin tarihi, 1968. İstanbul: Tifdruk Matbaacılık

VKVKBKM. 2022. Kültür Varlıklarının Envanter Bilgileri, Van Kültür Varlıklarını Koruma Bölge Kurulu Müdürlüğü Arşivi.